Serotonin receptor oligomerization regulates cAMP-based signaling

Sonal Prasad[1,2], Evgeni Ponimaskin[1,*], Andre Zeug[1,*]

[1] Cellular Neurophysiology, Center of Physiology, Hannover Medical School, Carl-Neuberg-Straße 1, 30625 Hannover, Germany

[2] Present address: Department of Clinical and Experimental Medicine, Linköping University, 581 83 Linköping, Sweden

* corresponding author

email: Zeug.Andre@mh-hannover.de

KEYWORDS: G-protein coupled receptor (GPCR), 5-HT_7R, 5-HT_{1A}R, Hetero-oligomerization, Förster Resonance Energy Transfer (FRET), cAMP signaling, Epac, Lux-FRET, Stoichiometry, Quantitative confocal microscopy.

JCS Advance Online Article. Posted on 1 August 2019

SUMMARY STATEMENT

The method developed in this study addresses the impact of GPCR hetero-oligomerization on downstream signaling and contributes to the identification of the stoichiometry of endogenously expressed GPCRs under physiological conditions.

ABSTRACT

Protein-protein interaction is often investigated using quantitative molecular microscopy with Förster Resonant Energy Transfer (FRET). We combined 'linear unmixing FRET' (lux-FRET) with the simultaneous application of a FRET-based biosensor for cAMP to investigate the oligomerization between the 5-HT_7 receptor (5-HT_7R) and the 5-HT_{1A} receptor (5-HT_{1A}R) and its importance for cAMP signaling. We found that the 5-HT_7R not only stimulates cAMP production, but also forms hetero-oligomers with 5-HT_{1A}R, which blocks the inhibitory effect of the latter. 5-HT_7R signaling however is not affected by this hetero-oligomerization. By modeling the kinetics of intracellular cAMP level changes in relation to the 5-HT_7R:5-HT_{1A}R stoichiometry we were able to decipher the complex signaling characteristics of endogenous serotonin receptors in cultured hippocampal neurons. Our findings indicate that the serotonergic signaling is not only modulated by the concentration of an individual receptor but also by its specific interaction with other receptors in endogenous systems. We conclude that the regulated ratio of serotonin receptors in immature and mature neurons may be critically involved in both the onset and response to treatments of psychiatric diseases such as anxiety and depression.

INTRODUCTION

G protein-coupled receptors (GPCRs) are a large protein superfamily of transmembrane receptors. They are known to be able to activate multiple downstream signaling modules (Marinissen and Gutkind, 2001; Woehler and Ponimaskin, 2009), which mediate a wide range of physiological processes. The mechanisms of several pathologies, including hypertension and neuropsychiatric disorders, are linked to dysregulations of GPCR signaling. Therefore, GPCRs are considered major targets for therapeutic intervention. Approximately 35% of all current drugs on the market act on the members of the GPCR family (Hauser et al., 2018). Nevertheless, the complexity of the underlying mechanisms that regulate the multimodal GPCR-mediated signaling remains poorly understood. In addition to the direct GPCR signaling, the formation of GPCR oligomers can affect various aspects of GPCR function. GPCR heteromerization was first proposed by Zoli *et al.* (Zoli et al., 1993) and later confirmed by Marshall *et al.*, who reported that the two nonfunctional GPCR monomers, GABAB1R and GABAB2R, can assemble in a signaling heterodimer at the cell surface (Marshall et al., 1999). GPCRs can form homo- and hetero-oligomers (Bulenger et al., 2005), whereas hetero-oligomers were found between partners of the same family (Panetta and Greenwood, 2008; Woehler et al., 2008), as well as between different classes of GPCRs (Trifilieff et al., 2011).

Accumulating evidence indicates that the dynamic formation of GPCR oligomer actively regulates all aspects of GPCR function, including synthesis, ligand binding, G-protein coupling, receptor trafficking and internalization (Borroto-Escuela et al., 2017; Milligan, 2007). The clinical significance of GPCR oligomerization has also become more evident during recent years, leading to the identification of receptor oligomers as novel therapeutic targets (Holliday et al., 2012; Milligan et al., 2014). For their directed application, the relative GPCR concentration of monomers, homomers and heteromers in endogenous systems must be identified. Particularly because of the absence of suitable methodology, this dynamic information must still be identified. However, this knowledge is of particular importance because heterodimers often possess distinct pharmacological or functional properties in comparison to monomers and homodimers (Rozenfeld and Devi, 2010).

To investigate the receptor complexes within the GPCR family, quantitative molecular microscopy provides a suitable toolbox to investigate these receptor-receptor interactions and obtain information in unprecedented detail (Prasad et al., 2013; Zeug et al., 2012). Fluorescence labeled GPCRs in combination with Förster Resonance Energy Transfer (FRET) based biosensors for second messengers have enabled the determination of kinetic parameters for various steps of GPCR signaling. We have shown that serotonin receptors type 7 (5-HT_7R) and type 1A (5-HT_{1A}R) can form homodimers (Kobe et al., 2008; Renner et

al., 2012; Woehler et al., 2008), as well as heterodimers (Renner et al., 2012), both *in vitro* and *in vivo*. Both 5-HTRs regulate the intracellular level of the second messenger cyclic AMP, although in the opposite direction: the activation of G_s via the 5-HT_7R results in increased production of cAMP (Adham et al., 1998; Wirth et al., 2017), while G_i activation via the 5-HT_{1A}R leads to a decrease in cAMP concentration (Albert et al., 1999; Kvachnina, 2005).

In experiments where 5-HT_7R and 5-HT_{1A}R were co-expressed, we found a heterogeneity of cAMP responses which could not be explained by the superposition of the counteracting 5-HTR signaling in respect to the receptor concentration. To identify the origin of this unexpected cAMP responses, we developed a highly relevant and clear but wide strategy to identify the impact of GPCR oligomerization on the downstream signaling. The approach is based on the simultaneous analysis of the receptor-receptor interaction and the receptor-mediated signaling in detail. To achieve that, 5-HT_7R and 5-HT_{1A}R were labeled with green and red fluorescent proteins allowing to quantify their oligomerization by applying the linear unmixing-FRET (lux-FRET) approach (Wlodarczyk et al., 2008; Zeug et al., 2012) to confocal microscopy. In parallel we determined the downstream signaling kinetics of the 5-HTRs by using FRET-based cAMP biosensor CEpac (Salonikidis et al., 2011).

In this study, we have characterized the downstream signaling kinetics of both 5-HTRs, first individually, and then in combination. To further identify the contribution of the individual 5-HTR we specifically blocked the counter effecting receptor and correlated the signaling kinetics with the hetero-oligomerization state of 5-HT_7R and 5-HT_{1A}R which let us identify that 5-HT_7R signaling is not disturbed upon hetero-oligomerization, while 5-HT_{1A}R signaling gets suppressed, the more it forms hetero-oligomers with 5-HT_7R. Here, a possible change in the 5-HT_{1A}R concentration could not explain the effect observed.

In the next step, we have shown that this advanced approach can be utilized to decipher the complex signaling characteristics of hippocampal neurons endogenously expressing serotonin receptors. From these findings, we were able to deduce the corresponding endogenous GPCR expression levels.

RESULTS

Agonist-specific effects on 5-HT$_{1A}$ and 5-HT$_7$ receptor-mediated cAMP signaling

To understand the complex signaling behavior in cells expressing heterodimers of 5-HT$_7$R and 5-HT$_{1A}$R, we first performed a detailed characterization of the cAMP responses mediated by the individual receptors. Thus, either 5-HT$_7$R-eGFP (Fig. 1A) or 5-HT$_{1A}$R-mCherry (Fig. 1D) were co-expressed with the FRET-based cAMP biosensor CEpac in N1E cells. The spectrally highly overlapping signals have been unmixed using the Zeiss LSM online fingerprinting mode (see methods). For receptor stimulation, we used serotonin (5-HT), as well as 5-CT and 8-OH-DPAT, which are known to be partial agonists for both receptor subtypes (Guscott et al., 2003; Guseva et al., 2014; Hedlund et al., 2004; Restrepo et al., 2010; Saxena and Lawang, 1985). The cAMP response was recorded at the single-cell level by monitoring the CEpac fluorescence intensity ratio of acceptor over donor (A/D ratio). From its amplitude and time dependence, the strength and speed of serotonergic signaling can be determined (Fig. S1A and Methods). In the absence of 5-HTR, no cAMP response was observed following treatment with agonists (Fig. S1C). In contrast, in cells that expressed 5-HT$_7$R, all three agonists were able to increase the intracellular cAMP level via G_s signaling, although with different efficiencies. When cells were pretreated with the highly specific 5-HT$_7$R antagonist SB-269970 (SB), the cAMP response was completely blocked. In contrast, pretreatment of cells with the 5-HT$_{1A}$R antagonist WAY100635 (WAY) did not produce an inhibitory effect (Fig. 1B). Statistical analysis by fitting the time dependence of the A/D ratio data to a single exponential fit model no1 (refer to Methods and Fig. S2A) revealed that 8-OH-DPAT had the significantly shortest activation time and the largest amplitude of the cAMP response (τ_1 = 25 ± 0.6 s, A_1 = -0.3 ± 0.005, N = 18, n = 438), compared with 5-HT (τ_1 = 74 ± 2.1 s, A_1 = -0.26 ± 0.006, N = 7, n = 204) and 5-CT (τ_1 = 42 ± 0.8 s, A_1 = -0.36 ± 0.007, N = 21, n = 561) (Fig. 1C, Movie S1). Thus, 8-OH-DPAT is a more efficient and potent agonist of the 5-HT$_7$R for the activation of the cAMP response than 5-CT and 5-HT.

We subsequently analyzed the ability of 5-HT$_{1A}$R-mediated signaling via G_i to inhibit the forskolin (FSK)-induced cAMP accumulation following receptor stimulation with 5-HT, 5-CT or 8-OH-DPAT. In all the cases, an increase of the A/D ratio of CEpac was observed, which indicated the 5-HT$_{1A}$R-mediated downregulation of intracellular [cAMP] (Fig. 1E, Movie S2). Pretreatment with the highly selective 5-HT$_{1A}$R antagonist WAY completely blocked this response, while [cAMP] was not affected by the application of the 5-HT$_7$R antagonist SB. Statistical evaluation of the time dependence of the A/D ratio data by the two exponential fit model no2 (refer to Methods and Fig. S2B) revealed a significantly shorter decay time for 5-CT (τ_2 = 110 ± 4 s, A_2 = 0.28 ± 0.01, N = 14, n = 328) than 5-HT (τ_2 = 150 ± 4 s,

A_2 = 0.26 ± 0.006, N = 6, n = 173) and 8-OH-DPAT (τ_2 = 240 ± 8 s, A_2 = 0.27 ± 0.009, N = 14, n = 312) responses, which shows 5-CT is a more efficient and potent 5-HT_{1A}R agonist than 8-OH-DPAT and 5-HT (Fig. 1F). It is noteworthy that in contrast to the 5-HT_7R, the amplitudes of the cAMP decay do not significantly vary between different agonists. Moreover, cAMP downregulation evoked by the 5-HT_{1A}R was a substantially slower process than cAMP upregulation by the 5-HT_7R (app. 4-fold slower, Fig. S3A, B).

Taken together, the results from these experiments emphasize on the CEpac biosensor as a sensible readout for the quantitative analysis of both cAMP stimulating and inhibiting signaling and identified 8-OH-DPAT and 5-CT as efficient agonists for the 5-HT_7R and 5-HT_{1A}R, respectively. The antagonist concentration of 10 µM applied 10 min prior to agonist treatment was found to specifically block the dedicated receptor function, while no unwanted cross-reaction was observed. (Fig. 1 and Fig. S1)

The effect of heterodimerization on 5-HT_{1A} receptor-mediated cAMP signaling

Having the knowledge of the individual signaling mechanism of 5-HT_7R and 5-HT_{1A}R, we can now address the question if the heterodimerization impacts the signaling of the individual 5-HTR or if the overall signaling is a simple superposition of both signaling cascades, which one would expect for the coexistence of monomers. To discover that, we co-expressed 5-HT_7R-eGFP and 5-HT_{1A}R-mCherry together with CEpac (Fig. 2A). Following the application of 8-OH-DPAT, which preferentially activates 5-HT_7R, a strong variation in the CEpac signal was observed (Fig. 2B, Movie S3), in which an increase of [cAMP] predominated. In contrast, following the application of 5-CT, a rather decreased [cAMP] was found, although the response also showed a strong variability (Fig. 2C, Movie S4). Statistical evaluation of the experimental data by double exponential fit model no3 (refer to Methods and Fig. S2C) did not provide a conclusive result due to the temporally and highly superimposing processes of cAMP up- and downregulation. Therefore, to investigate the individual receptor responses in cells co-expressing 5-HT_7R and 5-HT_{1A}R, we specifically blocked the counter effecting receptor via WAY and SB, respectively. When blocking the 5-HT_{1A}R with WAY, the 5-HT_7R mediated response to 8-OH-DPAT provides an upregulation of [cAMP] similar to that seen in the cells that only express the 5-HT_7R and CEpac (Fig. 2D, E, Movie S5, compare Fig. 1B). In contrast, blocking of the 5-HT_7R with SB lead to a significant reduction of the expected downregulation of the FSK-induced cAMP accumulation by 5-HT_{1A}R activation via G_i with 5-CT (Fig. 2F, G, Movie S6, compare Fig. 1F). Still, a strong heterogeneity from cell to cell was observed which is reflected in the large error-value in the statistical analysis of the response amplitudes (A_2 = 0.55 ± 0.30, N = 11, n = 251) compared to the system that only expressed 5-HT_{1A}R and CEpac (A_2 = 1.0 ± 0.02, N = 14, n = 328). Similar experiments of specifically blocking one 5-

HTR and stimulating the co-expressed counteracting 5-HTR with the three partial agonists have been performed. The fit results of the A/D ratio traces are shown through scatter correlation plots and their statistical evaluation (Fig. S3).

Correlation of cAMP response with relative expression levels of 5-HT$_7$R and 5-HT$_{1A}$R

To identify the source of the strong variation of cAMP responses in these experiments, we analyzed the relative expression levels and the levels of interaction of both 5-HT$_7$R and 5-HT$_{1A}$R by employing quantitative lux-FRET in parallel with cAMP responses (acquisition scheme, refer to Fig. S4). We subsequently found variations in the relative expression levels within the field of view in the range of ratio 4:1 to 1:4 (Fig. 3A, B). In line with Renner *et al*. (Renner et al., 2012), we could show the dependency between the donor molar fraction and apparent FRET efficiency in a pixel-based application. By fitting the dimerization model described in Renner *et al.*, relative dissociation constants in the order of $K_{1A\text{-}1A} > K_{1A\text{-}7} > K_{7\text{-}7}$ (0.11 > 0.04 > 0.02) obtained with confocal microscopy confirm previous results in cuvette experiments (Renner et al., 2012). The x_D corrected mean FRET efficiency was found to be Ef_{DA50} = 7 ± 2% (n = 50). This emphasizes the accuracy of our lux-FRET approach in advanced confocal microscopy and supports the quality of our oligomerization studies at subcellular resolution.

More importantly, we obtained a correlation between the cAMP response, receptor stoichiometry and oligomerization state, expressed as a donor molar fraction x_D, and the apparent FRET efficiencies Ef_D and Ef_A from lux-FRET (Fig. 3C). The 5-HT$_{1A}$R cAMP signaling response amplitude was plotted as a function of x_D, expressed as 5-HT$_7$R:5-HT$_{1A}$R stoichiometry (Fig. 3D). The amplitudes of the 5-HT$_{1A}$R response (A_2 of fit model no2) were normalized to accurately compare the responses from different measurements. The mean of A_2 of all cells with x_D < 0.2 within each measurement was normalized to 1.0. The data were fitted with a linear function delivering intercept (1.10 ± 0.04) and slope (-1.13 ± 0.08). In contrast, no correlation between cAMP response and 5-HTR concentration was observed in the experiments with single 5-HTR expression.

The experimental data were evaluated as previously described (Prasad et al., 2013). No significant changes in the FRET parameters were observed during the experiment.

Estimating the extent of 5-HTR heterodimerization level from cAMP signaling in hippocampal neurons

We further expect to derive the 5-HT_7R:5-HT_{1A}R stoichiometry from the cAMP response in a similar manner by utilizing our newly found correlation of 5-HT_{1A}R cAMP signaling and 5-HTR stoichiometry to primary neurons expressing only endogenous and thus unlabeled 5-HTR. Primary cultures of mouse hippocampal neurons were transfected with CEpac using electroporation and lipofectamine for DIV2 and DIV12 measurements, respectively. Following FSK treatment, similar cAMP responses were observed up to a single spine level (Fig. 4A).

The cAMP response in WT neurons expressing CEpac was investigated by blocking the 5-HT_7R with SB, treating neurons with FSK-IBMX and stimulating with 5-CT. The cAMP responses in neurons at different developmental stages were obtained and are illustrated through characteristic traces in Fig. 4B. On measuring the cAMP response in DIV12 neurons, the observed amplitudes were relatively high (A_2 = 0.08 ± 0.006, N = 11, n = 135), and at DIV2, the amplitudes were significantly lower (A_2 = 0.05 ± 0.004, N = 2, n = 13). Representative traces are shown in Fig. 4Bi.

The cAMP response in the WT neurons following stimulation with 8-OH-DPAT while blocking 5-HT_{1A}R with WAY led to faster cAMP upregulation on DIV2 than on DIV12 (Fig. S6A). Upon blocking the 5-HT_7R with SB and through the stimulation of the 5-HTR with 8-OH-DPAT, the intracellular cAMP level did not change (Fig. S6B). In 5-HT_7R-KO neurons, application of 8-OH-DPAT while blocking the 5-HT_{1A}R with WAY did not lead to a significant cAMP level change (Fig. S6C), while WAY completely abolished the effect of 5-CT (Fig. S6D).

To adapt the model developed in N1E cells to neurons, it was mandatory to calibrate for the maximal cAMP responses to 5-HT_{1A}R stimulation, as the amplitudes observed in hippocampal culture were notoriously smaller. In 5-HT_7R-KO neurons, the cAMP responses to 5-HT_{1A}R stimulation was supposed to be not interfered and thus maximal. The inhibition of the FSK-induced cAMP accumulation after 5-CT application was more pronounced in the 5-HT_7R-KO than in the WT neurons (Fig. 4Bii). Similar cAMP responses were observed for DIV2 (A_2 = 0.086 ± 0.008, N = 2, n = 12) and DIV12 neurons (A_2 = 0.099 ± 0.006, N = 6, n = 53). For the calibration to minimal cAMP responses to the 5-HT_{1A}R, a stoichiometry of dominating 5-HT_7R was provided by a transient overexpression of 5-HT_7R-eGFP in WT neurons. Under this condition of blocking the 5-HT_{1A}R with SB, only transient inhibition of the FSK-induced cAMP accumulation after 5-CT application was observed, which lasted at most two minutes (Fig. 4Biii). This behavior is consistent with our observations obtained in N1E cells. Statistical analysis of the cAMP responses shown in Fig 4B is provided in Fig. 4C.

Applying our approximation from N1E cells and assuming a linear correlation of cAMP response amplitudes with receptor stoichiometry (compare Fig. 3D), the 5-HT_7R:5-HT_{1A}R stoichiometry was approximated in WT neurons from their cAMP response amplitudes (Fig. 4D). We found a 5-HT_7R:5-HT_{1A}R stoichiometry of approximately 3:2 at DIV2 (N = 4) and 1:4 at DIV12 (N = 12), which is in good correlation with previous studies (Kobe et al., 2012).

For control experiments, 5-HT_7R-KO neurons co-expressing CEpac and 5-HT_7R-eGFP were used and receptors expression levels in neurons for DIV2 and DIV 12 are shown in Fig. S5A. Endogenous distribution of 5-HT_{1A}R in WT and 5-HT_7R-KO, DIV12 mature neurons was determined by specific antibody labelling (Fig. S5B).

DISCUSSION

While the concept of GPCR oligomerization has moved from a hypothesis to a well-accepted phenomenon, there remains a need to find a consensus on the importance of the physiological relevance and the potential pharmacological applicability of this phenomenon. Currently, FRET is extensively used to investigate GPCR oligomerization in live cells. In addition, various FRET-based biosensors have been successfully applied to study multiple intracellular signaling processes. However, methods to simultaneously investigate the GPCR complex stoichiometry and receptor-mediated signaling in their cellular context still remains undetermined. In this work, we have utilized FRET to measure cAMP dynamics in living cells with the CEpac biosensor (Salonikidis et al., 2011) while simultaneously measuring the 5-HT_7R-5-HT_{1A}R hetero-oligomerization level using the quantitative lux-FRET approach (Prasad et al., 2013; Wlodarczyk et al., 2008).

5-HT receptor mediated cAMP response for quantitative screening

The cAMP response of the CEpac biosensor enabled us to specifically compare the signaling of different agonists and antagonists and allowed us to record pharmacological responses in a highly reproducible manner, which may be used to facilitate high throughput screenings for new agonists and antagonists. Here, we exemplarily show the specificity of known agonists for 5-HT_7R and 5-HT_{1A}R: 5-HT, 5-CT and 8-OH-DPAT (Guscott et al., 2003; Guseva et al., 2014; Hedlund et al., 2004; Restrepo et al., 2010; Saxena and Lawang, 1985). 8-OH-DPAT was initially found as a specific agonist for the 5-HT_{1A}R (Hall et al., 1985; Middlemiss, 1984; Middlemiss and Fozard, 1983), and in line with the discovery of the 5-HT_7R subtype, it was also found to activate the 5-HT_7R (Lovenberg et al., 1993). In behavioral studies that had investigated the recovery after experimental traumatic brain injury in rats, Yelleswarapu *et al.* found that the induced cognitive benefits after the injury may be mediated more by the affinity of 8-OH-DPAT to 5-HT_7R than to 5-HT_{1A}R (Yelleswarapu et al., 2012). However, in subsequent rat behavioral studies, 8-OH-DPAT was discussed to stimulate 5-HT_{1A}R neglecting its affinity to 5-HT_7R (Clissold et al., 2013). We found that the 8-OH-DPAT induces a stronger 5-HT_7R mediated cAMP response than 5-CT and 5-HT (1.7x and 3x faster, respectively). In contrast, 5-CT was found to be a more potent agonist of 5-HT_{1A}R (1.4x faster than with 5-HT and 2.2x faster than with 8-OH-DPAT stimulation). This approach also enabled us to obtain a time dependent dose response curve for the specific 5-HTR antagonists SB (Lovell et al., 2000) and WAY (Fornal et al., 1996) for the 5-HT_7R and 5-HT_{1A}R, respectively.

Functional role of heterodimerization

Although the existence of GPCR hetero-oligomers has become generally accepted, their physiological evidence in endogenous systems, such as neurons, as well as their functional importance remain a matter of debate (Trifilieff et al., 2011). In a recent study, we have shown that the 5-HT_7R and 5-HT_{1A}R can form homo- and hetero-oligomers (Renner et al., 2012). Considering the antagonistic action of the 5-HT_7R and 5-HT_{1A}R in regulating the cAMP concentration, the question arose about the specific functional impact of the formation of hetero- over homo-oligomers. This is of particular importance because the balance of the expression level of the 5-HT_7R and 5-HT_{1A}R, and thus the balance between the homo- and hetero-oligomer formation, changes during the neuronal development (Kobe et al., 2012; Rojas et al., 2017), which could provide further downstream regulatory consequences. Therefore, we co-expressed 5-HT_7R and 5-HT_{1A}R together with CEpac in various 5-HT_7R:5-HT_{1A}R plasmid concentration ratios to investigate the downstream signaling in relation to 5-HTR oligomerization.

While obtaining the cAMP response, we simultaneously monitored the oligomerization state of the 5-HTR with the lux-FRET technique in confocal microscopy (Prasad et al., 2013; Wlodarczyk et al., 2008; Zeug et al., 2012). We have shown that on a single-cell level, the change in 5-HT_7R:5-HT_{1A}R stoichiometry correlates with the level of hetero-oligomer formation. From the heterogeneity of 5-HTR expression levels of cells expressing both receptors together with CEpac (Fig. 3A,B), we could obtain the relative binding affinities of 5-HT_7R and 5-HT_{1A}R homo- and heterodimers (Fig. 3C), which are in line with the results obtained from the fluorescence spectrometer measurements of lysed N1E cell ensembles in cuvettes (Renner et al., 2012). Given that the majority of GPCRs appear to form oligomers constitutively, the addition of an agonist could result in changes in the oligomerization state (Kaczor et al., 2013). By comparing lux-FRET measurements before and after the treatment, we could clarify that the specific activation of the 5-HTR does not influence their oligomerization state.

To assess the diversity in cAMP responses when co-expressing 5-HT_7R and 5-HT_{1A}R, we have monitored the cAMP signaling while specifically blocking the 5-HT_7R and 5-HT_{1A}R with SB and WAY, respectively, prior to stimulating with agonists. By specifically blocking the 5-HT_7R with SB and stimulating with 5-CT (Fig. 2F, G), we found that in cells with a 5-HT_7R:5-HT_{1A}R stoichiometry shifted towards the 5-HT_7R, and the 5-HT_{1A}R mediated cAMP signaling becomes increasingly suppressed. This correlation could not be simply explained by the relatively low 5-HT_{1A}R concentration, as in experiments with cells expressing single 5-HT_{1A}R, where no correlation was identified between the cAMP response and 5-HT_{1A}R

concentration (cf. Fig. 1F and 2E). Taking into account the finding that the more the 5-HT_7R:5-HT_{1A}R stoichiometry is shifted towards the 5-HT_7R, the more it forms oligomers with 5-HT_{1A}R (Renner et al., 2012). This interaction can explain the observed reduction in the cAMP downregulation. From the correlation identified between the ratio of hetero-oligomerization and the extent of the receptor-mediated cAMP response (Fig. 3C), we developed a model which suggests that the 5-HT_{1A}R activated G_i signaling is blocked upon 5-HT_7R–5-HT_{1A}R heterodimer formation (Fig. 5). However, 5-HT_7R mediated cAMP signaling via G_s is not influenced by the heterodimer formation with the 5-HT_{1A}R. Due to the experimental design we cannot identify the source of this behavior, such as if the hetero-oligomerization impacts agonist binding or specific G protein coupling.

These findings indicate a strong impact of GPCR oligomerization on the downstream signaling and thus on the functional consequences and regulatory effects of GPCR oligomerization. Functional consequences have been extensively studied for adenosine A_{2A}–dopamine D_2 receptor heteromers (Azdad et al., 2008; Ferre et al., 1991). For the adenosine A_{2A} receptor, the affinity of its selective agonist SCH 442416 is decreased when A2AR forms heteromers with the dopamine D2 receptor, but not when it forms homodimers (Orru et al., 2011). For further examples, refer to (Gurevich and Gurevich, 2008; Milligan et al., 2007).

Determination of stoichiometry for endogenously expressed receptors

It is notoriously challenging to obtain naïve expression levels of endogenous proteins in live cell experiments. By employing our protocol optimized for cAMP measurements in N1E cells co-expressing 5-HTR (Fig. S4), we were able to explore the extent of oligomerization between the endogenously expressed 5-HT_7R and 5-HT_{1A}R in a primary culture of hippocampal neurons deduced from their cAMP response. Compared to the experiments in N1E cells, the expression level of transiently expressed CEpac in hippocampal neurons is rather moderate and particularly faint in regions of neuronal protrusions. The signal-to-noise ratio of the biosensor readout is therefore lower than in experiments in N1E cells (Fig. 4A). As the cAMP response on FSK stimulation indicated similar responses in different parts of the hippocampal neurons, transiently transfected with CEpac, we decided to monitor 5-HTR mediated signaling from somatic regions mostly. The observed amplitudes were analogous to the FSK treatment of N1E cells (cf. Fig. 1E and 4A).

We have found deviating cAMP responses in neurons at different developmental stages. In DIV2 neurons, the 5-HT_{1A}R mediated cAMP response was significantly lower than in the observations in DIV12 neurons (Fig. 4B and C). From our previous finding in N1E cells, we can explain this finding by the specific inhibitory impact of 5-HT_7R–5-HT_{1A}R heterodimerization

on the 5-HT_{1A}R mediated cAMP signaling. The obtained estimates of 5-HT_7R:5-HT_{1A}R stoichiometry at DIV2 and DIV12 investigated here are in good correlation with our previous findings, in which the 5-HT_7R expression is downregulated at a later developmental stage, while the 5-HT_{1A}R expression is consistent as shown on a mRNA level (Kobe et al., 2012).

As a primary outcome from this study, it was shown that the coordinated changes in the expression of 5-HT_7R and 5-HT_{1A}R during neuronal maturation *in vitro* are critically involved in the regulation of receptor functions. This finding suggests that unless 5-HT_{1A}R expression remains consistent, cAMP is not down regulated as efficiently in the early stages than in the later developmental stages.

In addition to the well-known cAMP signaling, 5-HT_7Rs can couple to the G_{12}-protein, which activates small GTPases of the Rho family and leads to enhanced neurite outgrowth, synaptogenesis and neuronal excitability (Kvachnina, 2005; Woehler and Ponimaskin, 2009). Whether that pathway is influenced by hetero-oligomerization with 5-HT_{1A}Rs it has not been previously investigated. This may soon be a potent area of scientific research by applying our double FRET concept.

Taken together, our present results indicate a general possibility that the downstream signaling dynamics in cells may be used as a quantitative read-out for the analysis of receptor–receptor interactions. Given that this particular method does not require labeling of oligomerization components, we are able to obtain the stoichiometry of the receptor and level of receptor expression *in vivo* at different developmental stages. This could be very important for drug discovery in the specific targeting of receptors and further treatment of diseases related to serotonin receptors.

MATERIALS AND METHODS

Reagents

Solutions were used if not mentioned others: 5-HT hydrochloride (H9523 Sigma, Munich, Germany), 5-CT maleate (0458 Tocris Bioscience, Wiesbaden-Nordenstadt, Germany) and 8-OH-DPAT hydrobromide (0529 Tocris Bioscience, Wiesbaden-Nordenstadt, Germany): 10 µM in ddH_2O; Forskolin (FSK, F-9929 LC lab): 5 µM in DMSO; IBMX (I5897 Sigma, Munich, Germany): 50 µM in DMSO; SB-269970 hydrochloride (SB; 1612 Tocris Bioscience, Wiesbaden-Nordenstadt, Germany): 100 nM in ddH_2O; WAY maleate (WAY; 4380 Tocris Bioscience, Wiesbaden-Nordenstadt, Germany): 10 nM in ddH_2O. Furthermore, we used Anti-5-HT_{1A}R rabbit polyclonal (ASR-021 Alomone labs, Jerusalem, Israel); Alexa Fluor 594-AffiniPure Donkey Anti-Rabbit IgG (H+L) (711-585-152 Jackson ImmunoResearch, Cambridgeshire, UK); PFA-Paraformaldehyde (0335.3); BSA-Bovine Serum Albumin (8076.3); and D+Sucrose (4621.1) were obtained from Roth, Karlsruhe, Germany and FBS-Fetal Bovine Serum (10270-106 Life Technologies, Darmstadt, Germany).

Construction of 5-HT_7-eGFP and 5-HT_{1A}-mCherry plasmids

The plasmids of 5-HT_7R-eGFP and 5-HT_{1A}R-mCherry were designed with a PCR-based approach. eGFP and mCherry were fused to the N-terminal site of the 5-HT_7R and 5-HT_{1A}R, respectively (Table S1). All constructs were sequenced. The empty vector (pcDNA3.1) and cAMP biosensor (CEpac) plasmids have previously been described (Salonikidis et al., 2011). pBABE-puro mCherry-eGFP-LC3B (Addgene #22418) was used as an eGFP-mCherry tandem construct for lux-FRET measurement and calibration.

Cell culture and transfection

Cell culturing of murine N1E-115 neuroblastoma (N1E) cells (American Type Culture Collection), which are known not to express any G-protein coupled 5-HTR (Richelson, 1990), was described elsewhere (Renner et al., 2012). Cells were plated on 18 mm glass coverslips and transfected using Lipofectamine 2000 reagent (Life Technologies, Darmstadt, Germany) according to the manufacturer's instruction. Plasmid amount was optimized to 5-HT_7R-eGFP: 0.3 µg, 5-HT_{1A}R-mCherry: 0.3 µg, CEpac: 1.4 µg maintaining 2 µg in total. For experiments that required single or double plasmids, pcDNA3.1 was used. The extracellular salt solution (ESS) used for N1E cells contained NaCl:150, KCl:5, $CaCl_2.2H_2O$:2, $MgCl_2.6H_2O$:1, HEPES:10 (all mM), pH 7.4 and 342 mOsmol.

Animals and neuronal preparation

Primary murine hippocampal neuronal cultures were prepared from postnatal day 1 or 2 (P1 or P2) old mouse, both genders, of WT (C57BL6/J) and 5-HT_7R-KO mice (B6.129-*Htr7*^{tm1Sut}/J, JAX:019453) as previously described (Dityateva et al., 2003) with a slight modification in the protocol. After hippocampal isolation and preparation, the cells were plated onto Poly-D-Lysine hydrobromide (PLL)-coated glass 18-mm coverslips and grown in NBA medium containing (P/S, B-27 supplement and Glutamax) at 37°C, 5% CO_2. On day *in vitro* (DIV) 0: primary hippocampal neuronal cells in suspension were electroporated with CEpac using a Primary Cell Nucleofector kit (Lonza, Köln, Germany); DIV 7: primary cells were transfected with the CEpac plasmids. Measurements were performed on DIV 2 and DIV12. The transfection mix was removed after 1 h, and cells were incubated for the following days in NBA medium. The physiological saline solution used for neurons contained NaCl:119, KCl:5, $CaCl_2.2H_2O$:2, $MgCl_2.6H_2O$:2, HEPES:25 (all mM), pH 7.4 and 342 mOsmol.

Confocal laser scanning microscopy: ratiometric cAMP and lux-FRET measurements in living cells

Confocal imaging was performed after comprehensive calibration of the system according to (Butzlaff et al., 2015; Prasad et al., 2013). N1E cells were subjected to fluorescence ratio time series measurements and, in experiments with co-expression of both 5-HTRs, to lux-FRET imaging (Fig. S4). Given that lux-FRET requires alternating excitation with two wavelengths and is thus sensitive to special overlap, z-stacks were obtained to allow shift correction in 3D and capture the same optical level of the image during and after the time series experiments. Cells from culture medium were transferred in ESS at room temperature prior to the time series and lux-FRET microscopy experiments. All data were acquired on a Zeiss LSM 780 controlled with ZEN 2012 software. The following acquisition configuration was used: 40x/1.2 NA water immersion objective, bit depth 16-bit, and pinhole of 1.7 AU at zoom 0.6.

Monitoring cAMP responses with the FRET-based biosensor CEpac

An optimized variant of the EPAC biosensor (Salonikidis et al., 2011) was used to monitor changes in cAMP concentration during time series measurements. CEpac acts inverse, showing high FRET at low cAMP concentration and low FRET at high cAMP concentration (Fig. S1A). The standard ratiometric readout for FRET based biosensors, the acceptor / donor fluorescence ratio, (A/D ratio) does thus show a decrease in the A/D ratio upon increasing [cAMP]. Unless the A/D ratio shows apparently smaller amplitudes of ratio changes over the inverse, the donor / acceptor ratio, the A/D ratio was used to avoid division by small numbers

at low FRET. The resulting amplitudes from the exponential fit models (Fig. S2) must be red as cAMP increase for $A_1 < 0$ and a cAMP decrease for $A_2 > 0$.

Time series measurement for cAMP responses

CEpac biosensor and 5-HT_7R-eGFP were excited with a 440 nm laser line and 5 HT_{1A}R-mCherry with 561 nm (MBS 440, MBS 458/561, emission range 450 – 600 nm). Images were acquired at a frame size of 1024*1024 pixels and a frame acquisition time of 6.8 s. During the experiments, 100 cycles with 10 s intervals along with continuous refocusing using the Zeiss "Definite Focus" were used. The fluorescence spectra of Cerulean, mCitrine, eGFP and mCherry from single transfections acquired in lambda mode and background corrected were used as references for unmixing in the online fingerprinting mode. Cells that showed specific plasma membrane labeled with moderate 5-HT_7R and 5-HT_{1A}R and moderate cAMP biosensor expression were selected for analysis. In all time-series experiments, 18-20 frames (3.0 min) were captured prior to application. Agonists and antagonists were applied via a perfusion system (Warner Instruments) with a constant flow rate of 1.0 ml min^{-1}, thus enabling a complete exchange of solution within 1.0 min. The application protocol was adjusted by optimizing the agonist and antagonist concentrations and the blocking time. The working concentrations of 5-HT, 5-CT and 8-OH-DPAT were: 10 µM; SB: 100 nM; WAY: 10 nM; FSK: 5 µM; IBMX: 50 µM. Concentrations for FSK and IBMX were chosen to obtain cAMP increase high enough to show significant cAMP decrease by activating 5-HT_{1A}R, but low enough not to saturate the biosensor and not suppressing the 5-HT_{1A}R signaling. The blocking time was set to 10.0 min prior to agonists application. Quantitative FRET data evaluation was conducted offline. The intensities in all four colors were determined from whole cell regions of interest drawn manually at a higher magnification online in parallel to ongoing measurements.

Fitting models for A/D ratio time series data

Since 5-HT_7R and 5-HT_{1A}R are known to regulate the intracellular cAMP production upon activation, mathematical modelling was used to quantify the change in intracellular cAMP. Three fit models were developed to describe the time dependent changes in the cAMP concentration (Fig. S2): fit model no1 - a single exponential fit with a polynomial offset (*polyoff*), which delivers decay time τ_1 and amplitude A_1 starting at time point t_0; fit model no2 - two exponential fit with polynomial offset at two time points (t_1 and t_2), which delivers a set of two amplitude (A_1 and A_2) and decay time (τ_1 and τ_2) parameters for cAMP up and down regulation; and fit model no3 - a double exponential fit, which combines two biological processes at one time point. It also delivers two sets of parameters of amplitude and decay time values, where the real value of the decay time and amplitude cannot be deduced due to the complexities of

model fitting. Thus, raw data for the third type of response were simply fitted with the model, and the deduced quantities could rarely be used.

Lux-FRET measurement

Lux-FRET imaging was performed before and after the time series acquisition on N1E cells that expressed 5-HT_7R and 5-HT_{1A}R together with CEpac. Z-stacks (10 slices, 1.0 µm spacing) were acquired at 488 nm and 561 nm excitation, MBS 488/561, and an emission range 500-700 nm. All other acquisition settings were kept the same as previously stated. A schematic representation of the described measurement protocol and acquisition settings is shown in Fig. S4. For pixel-based analysis and to achieve a high spatial resolution in 3D in detail, the setup was calibrated according to (Butzlaff et al., 2015; Prasad et al., 2013). Alternating linewise switching excitation was achieved by a custom-tailored acquisition protocol generated by the LIC Macro toolbox (Roland Nitschke, Life Imaging Center, University of Freiburg, Germany). The laser power was set to 3% for 488 nm and 561 nm excitations to avoid bleaching. Images for reference were acquired from cells that expressed fluorophores separately; the eGFP-mCherry tandem construct was used in the experiment with the previously described acquisition settings for a single image. The correlation between FRET parameters and intensity was used to verify that receptor concentration related artifacts as 'molecular crowding' are avoided.

To correlate receptor oligomerization obtained by lux-FRET analysis with the serotonergic signaling obtained by cAMP kinetics, both properties have been obtained from all the ROIs (compare Fig. S4). Since lux-FRET does also provide relative concentrations of donor and acceptor, i.e. 5-HT_7R and 5-HT_{1A}R, it is possible to distinguish between the influence of oligomerization and concentration artefacts.

Data evaluation

Imaging data were evaluated offline using Matlab R2015a (the Mathworks, Natick, MA, USA, licensed MHH) scripts. To determine the FRET efficiency for 5 HT_7R - 5-HT_{1A}R heterodimers, we performed pixel basis lux-FRET analysis described in detail in (Prasad et al., 2013; Wlodarczyk et al., 2008). Data where shift and background corrected and extracted from manually drawn regions of interests (ROI) covering whole cell including plasma membrane. The standard error of the mean (s.e.m) was derived for all FRET quantities. The same ROIs drawn for the time series were used for the lux-FRET analysis. Three ratio models were applied to describe the time dependent changes in the cAMP concentration (Fig. S2). The fluorescence ratio signal was normalized to 1.0 by dividing the ratios of each trace by its emission ratio immediately before stimulation (*offset*).

Statistical analyses were performed in GraphPad Prism 8.0 (licensed LiU). The results are expressed as the mean ± s.e.m. Data were tested for significance with One-Way ANOVA with Bonferroni's Multiple Comparison test. Prism was used for illustration of the fluorescence ratio traces. The fluorescence images for N1E and hippocampal neurons were processed in ImageJ 1.49. Contour plots of the 2D histogram were generated in Matlab and statistically analyzed using OriginPro 2017 (licensed LiU).

Immunostaining and imaging

Co-localization studies were performed by labeling transfected DIV12 WT and 5-HT_7R-KO neurons. Cultured neurons were fixed with 4% PFA and 3% Sucrose (pH 7.4) for 10 min. The neurons were permeabilized with methanol at 4°C for 5 min, washed with PBS thrice before blocking for half an hour at RT with 2% BSA and Normal Donkey Serum (NDS 017-000-121, Jackson Immunoresearch, Cambridgeshire, UK) and 3% Sucrose in 10% FBS. Immunolabeling was subsequently performed with anti-5-HT_{1A}R as the primary antibody overnight at a 1:200 dilution and with Alexa Fluor 594 tagged secondary antibody for 1 h at 1:500 dilution, followed by a PBS washing step after each antibody labeling. Fluorescence images of mounted neurons were obtained with the LSM 780 in channel mode excited at 440 nm for Cerulean, mCitrine and eGFP fluorescence and at 561 nm for mCherry fluorescence and imaged with a 63x/1.4NA oil immersion objective.

Acknowledgements

The authors thank Roland Nitschke from Life Imaging Centre, University of Freiburg for providing LIC Macro toolbox.

Footnotes

Competing interests

The authors declare no conflict of competing interests.

Author contributions

Performed experiments, data acquisition and collection: S.P.; Data analysis and curation: S.P.; Data interpretation, statistical analysis and methodology: S.P., A.Z.; Study supervision and research design: A.Z., E.G.P.; Writing - original draft: S.P., A.Z.; Writing - review and editing: S.P., A.Z.

Funding

This study was supported by the Bundesministerium für Bildung und Forschung (BMBF, Federal Ministry of Education and Research, Germany, 0315690D to S.P. and A.Z.). A.Z. and E.G.P. were supported by the Deutsche Forschungsgemeinschaft (DFG, German Research Foundation, ZE994/2, PO732 and SFB621/C12).

Abbreviations

5-CT,	5-Carboxamidotryptamine
5-HT,	Serotonin
5-HT_{1A}R,	Serotonin receptor subtype 1A
5-HT_7R,	Serotonin receptor subtype 7
5-HT_7R-KO,	5-HT_7R knock out
5-HTR,	Serotonin receptor
8-OH-DPAT,	8-Hydroxy-2-dipropylaminotetralin
BSA,	Bovine Serum Albumin;
cAMP,	Cyclic adenosine mono phosphate;
CEpac,	Cerulean/Citrine tagged exchange protein activated by cAMP;
DIV,	Day *in vitro*
FBS,	Fetal Bovine Serum.
FRET	Förster Resonance Energy Transfer
FSK,	Forskolin;
GABABR	Gamma-aminobutyric acid B receptor
GPCR	G-protein coupled receptor
IBMX,	3-Isobutyl-1-methylxanthine;
lux-FRET,	linear unmixing FRET;
NDS,	Normal Donkey Serum;
PFA,	Paraformaldehyde;
PLL,	Poly-D-Lysine;
WT,	Wild type

REFERENCES

Adham, N., Zgombick, J. M., Bard, J. and Branchek, T. A. (1998). Functional Characterization of the Recombinant Human 5-Hydroxytryptamine7(a) Receptor Isoform Coupled to Adenylate Cyclase Stimulation. *J. Pharmacol. Exp. Ther.* **287**, 508–514.

Albert, P. R., Sajedi, N., Lemonde, S. and Ghahremani, M. H. (1999). Constitutive Gi2-dependent Activation of Adenylyl Cyclase Type II by the 5-HT1A Receptor INHIBITION BY ANXIOLYTIC PARTIAL AGONISTS. *J. Biol. Chem.* **274**, 35469–35474.

Azdad, K., Gall, D., Woods, A. S., Ledent, C., Ferré, S. and Schiffmann, S. N. (2008). Dopamine D2 and Adenosine A2A Receptors Regulate NMDA-Mediated Excitation in Accumbens Neurons Through A2A–D2 Receptor Heteromerization. *Neuropsychopharmacology* **34**, 972–986.

Borroto-Escuela, D. O., Carlsson, J., Ambrogini, P., Narváez, M., Wydra, K., Tarakanov, A. O., Li, X., Millón, C., Ferraro, L., Cuppini, R., et al. (2017). Understanding the Role of GPCR Heteroreceptor Complexes in Modulating the Brain Networks in Health and Disease. *Front. Cell. Neurosci.* **11**,.

Bulenger, S., Marullo, S. and Bouvier, M. (2005). Emerging role of homo- and heterodimerization in G-protein-coupled receptor biosynthesis and maturation. *Trends Pharmacol. Sci.* **26**, 131–137.

Butzlaff, M., Weigel, A., Ponimaskin, E. and Zeug, A. (2015). eSIP: A Novel Solution-Based Sectioned Image Property Approach for Microscope Calibration. *PLoS ONE* **10**, e0134980.

Clissold, K. A., Choi, E. and Pratt, W. E. (2013). Serotonin 1A, 1B, and 7 receptors of the rat medial nucleus accumbens differentially regulate feeding, water intake, and locomotor activity. *Pharmacol. Biochem. Behav.* **112**, 96–103.

Dityateva, G., Hammond, M., Thiel, C., Ruonala, M. O., Delling, M., Siebenkotten, G., Nix, M. and Dityatev, A. (2003). Rapid and efficient electroporation-based gene transfer into primary dissociated neurons. *J. Neurosci. Methods* **130**, 65–73.

Ferre, S., Euler, G. von, Johansson, B., Fredholm, B. B. and Fuxe, K. (1991). Stimulation of high-affinity adenosine A2 receptors decreases the affinity of dopamine D2 receptors in rat striatal membranes. *Proc. Natl. Acad. Sci.* **88**, 7238–7241.

Fornal, C. A., Metzler, C. W., Gallegos, R. A., Veasey, S. C., McCreary, A. C. and Jacobs, B. L. (1996). WAY-100635, a potent and selective 5-hydroxytryptamine1A antagonist, increases serotonergic neuronal activity in behaving cats: comparison with (S)-WAY-100135. *J. Pharmacol. Exp. Ther.* **278**, 752–762.

Gurevich, V. V. and Gurevich, E. V. (2008). How and why do GPCRs dimerize? *Trends Pharmacol. Sci.* **29**, 234–240.

Guscott, M. R., Egan, E., Cook, G. P., Stanton, J. A., Beer, M. S., Rosahl, T. W., Hartmann, S., Kulagowski, J., McAllister, G., Fone, K. C. F., et al. (2003). The hypothermic effect of 5-CT in mice is mediated through the 5-HT7 receptor. *Neuropharmacology* **44**, 1031–1037.

Guseva, D., Wirth, A. and Ponimaskin, E. (2014). Cellular mechanisms of the 5-HT7 receptor-mediated signaling. *Front. Behav. Neurosci.* **8**, 306.

Hall, M. D., Mestikawy, S. E., Emerit, M. B., Pichat, L., Hamon, M. and Gozlan, H. (1985). [3H]8-Hydroxy-2-(Di-n-Propylamino)Tetralin Binding to Pre- and Postsynaptic 5-Hydroxytryptamine Sites in Various Regions of the Rat Brain. *J. Neurochem.* **44**, 1685–1696.

Hauser, A. S., Chavali, S., Masuho, I., Jahn, L. J., Martemyanov, K. A., Gloriam, D. E. and Babu, M. M. (2018). Pharmacogenomics of GPCR Drug Targets. *Cell* **172**, 41-54.e19.

Hedlund, P. B., Kelly, L., Mazur, C., Lovenberg, T., Sutcliffe, J. G. and Bonaventure, P. (2004). 8-OH-DPAT acts on both 5-HT1A and 5-HT7 receptors to induce hypothermia in rodents. *Eur. J. Pharmacol.* **487**, 125–132.

Holliday, N. D., Watson, S.-J. and Brown, A. J. H. (2012). Drug discovery opportunities and challenges at G protein coupled receptors for long chain free fatty acids. *Mol. Struct. Endocrinol.* **2**, 112.

Kaczor, A. A., Selent, J. and Poso, A. (2013). Chapter 5 - Structure-Based Molecular Modeling Approaches to GPCR Oligomerization. In *Methods in Cell Biology* (ed. Conn, P. M.), pp. 91–104. Academic Press.

Kobe, F., Renner, U., Woehler, A., Wlodarczyk, J., Papusheva, E., Bao, G., Zeug, A., Richter, D. W., Neher, E. and Ponimaskin, E. (2008). Stimulation- and palmitoylation-dependent changes in oligomeric conformation of serotonin 5-HT1A receptorsi. *Biochim. Biophys. Acta BBA - Mol. Cell Res.* **1783**, 1503–1516.

Kobe, F., Guseva, D., Jensen, T. P., Wirth, A., Renner, U., Hess, D., Müller, M., Medrihan, L., Zhang, W., Zhang, M., et al. (2012). 5-HT7R/G12 Signaling Regulates Neuronal Morphology and Function in an Age-Dependent Manner. *J. Neurosci.* **32**, 2915–2930.

Kvachnina, E. (2005). 5-HT7 Receptor Is Coupled to G Subunits of Heterotrimeric G12-Protein to Regulate Gene Transcription and Neuronal Morphology. *J. Neurosci.* **25**, 7821–7830.

Lovell, P. J., Bromidge, S. M., Dabbs, S., Duckworth, D. M., Forbes, I. T., Jennings, A. J., King, F. D., Middlemiss, D. N., Rahman, S. K., Saunders, D. V., et al. (2000). A Novel, Potent, and Selective 5-HT7 Antagonist: (R)-3-(2-(2-(4-Methylpiperidin-1-yl)ethyl)pyrrolidine-1-sulfonyl)phenol (SB-269970). *J. Med. Chem.* **43**, 342–345.

Lovenberg, T. W., Baron, B. M., de Lecea, L., Miller, J. D., Prosser, R. A., Rea, M. A., Foye, P. E., Racke, M., Slone, A. L., Siegel, B. W., et al. (1993). A novel adenylyl

cyclase-activating serotonin receptor (5-HT7) implicated in the regulation of mammalian circadian rhythms. *Neuron* **11**, 449–458.

Marinissen, M. J. and Gutkind, J. S. (2001). G-protein-coupled receptors and signaling networks: emerging paradigms. *Trends Pharmacol. Sci.* **22**, 368–376.

Marshall, F. H., White, J., Main, M., Green, A. and Wise, A. (1999). GABAB receptors function as heterodimers. *Biochem. Soc. Trans.* **27**, 530–535.

Middlemiss, D. N. (1984). 8-Hydroxy-2-(di-n-propylamino) tetralin is devoid of activity at the 5-hydroxytryptamine autoreceptor in rat brain. Implications for the proposed link between the autoreceptor and the [3H] 5-HT recognition site. *Naunyn. Schmiedebergs Arch. Pharmacol.* **327**, 18–22.

Middlemiss, D. N. and Fozard, J. R. (1983). 8-Hydroxy-2-(di-n-propylamino)-tetralin discriminates between subtypes of the 5-HT1 recognition site. *Eur. J. Pharmacol.* **90**, 151–153.

Milligan, G. (2007). G protein-coupled receptor dimerisation: Molecular basis and relevance to function. *Biochim. Biophys. Acta BBA - Biomembr.* **1768**, 825–835.

Milligan, G., Canals, M., Pediani, J. D., Ellis, J. and Lopez-Gimenez, J. F. (2007). The Role of GPCR Dimerisation/Oligomerisation in Receptor Signalling. In *GPCRs: From Deorphanization to Lead Structure Identification*, pp. 145–162. Springer, Berlin, Heidelberg.

Milligan, G., Ulven, T., Murdoch, H. and Hudson, B. D. (2014). G-protein-coupled receptors for free fatty acids: nutritional and therapeutic targets. *Br. J. Nutr.* **111**, S3–S7.

Orru, M., Bakešová, J., Brugarolas, M., Quiroz, C., Beaumont, V., Goldberg, S. R., Lluís, C., Cortés, A., Franco, R., Casadó, V., et al. (2011). Striatal Pre- and Postsynaptic Profile of Adenosine A2A Receptor Antagonists. *PLoS ONE* **6**, e16088.

Panetta, R. and Greenwood, M. T. (2008). Physiological relevance of GPCR oligomerization and its impact on drug discovery. *Drug Discov. Today* **13**, 1059–1066.

Prasad, S., Zeug, A. and Ponimaskin, E. (2013). Chapter 14 - Analysis of Receptor–Receptor Interaction by Combined Application of FRET and Microscopy. In *Methods in Cell Biology* (ed. Conn, P. M.), pp. 243–265. Academic Press.

Renner, U., Zeug, A., Woehler, A., Niebert, M., Dityatev, A., Dityateva, G., Gorinski, N., Guseva, D., Abdel-Galil, D., Fröhlich, M., et al. (2012). Heterodimerization of serotonin receptors 5-HT1A and 5-HT7 differentially regulates receptor signalling and trafficking. *J. Cell Sci.* **125**, 2486–2499.

Restrepo, B., Martín, M. L., San Román, L. and Morán, A. (2010). Peripheral 5-HT 1A and 5-HT 7 Serotonergic Receptors Modulate Parasympathetic Neurotransmission in Long-Term Diabetic Rats. *J. Diabetes Res.*

Richelson, E. (1990). The Use of Cultured Cells in the Study of Mood-Normalizing Drugs. *Pharmacol. Toxicol.* **66**, 69–75.

Rojas, P. S., Aguayo, F., Neira, D., Tejos, M., Aliaga, E., Muñoz, J. P., Parra, C. S. and Fiedler, J. L. (2017). Dual effect of serotonin on the dendritic growth of cultured hippocampal neurons: Involvement of 5-HT1A and 5-HT7 receptors. *Mol. Cell. Neurosci.* **85**, 148–161.

Rozenfeld, R. and Devi, L. A. (2010). Receptor heteromerization and drug discovery. *Trends Pharmacol. Sci.* **31**, 124–130.

Salonikidis, P. S., Niebert, M., Ullrich, T., Bao, G., Zeug, A. and Richter, D. W. (2011). An Ion-insensitive cAMP Biosensor for Long Term Quantitative Ratiometric Fluorescence Resonance Energy Transfer (FRET) Measurements under Variable Physiological Conditions. *J. Biol. Chem.* **286**, 23419–23431.

Saxena, P. R. and Lawang, A. (1985). A comparison of cardiovascular and smooth muscle effects of 5-hydroxytryptamine and 5-carboxamidotryptamine, a selective agonist of 5-HT1 receptors. *Arch. Int. Pharmacodyn. Thérapie* **277**, 235–252.

Trifilieff, P., Rives, M.-L., Urizar, E., Piskorowski, R. A., Vishwasrao, H. D., Castrillon, J., Schmauss, C., Slättman, M., Gullberg, M. and Javitch, J. A. (2011). Detection of antigen interactions ex vivo by proximity ligation assay: endogenous dopamine D2-adenosine A2A receptor complexes in the striatum. *BioTechniques* **51**, 111–118.

Wirth, A., Holst, K. and Ponimaskin, E. (2017). How serotonin receptors regulate morphogenic signalling in neurons. *Prog. Neurobiol.* **151**, 35–56.

Wlodarczyk, J., Woehler, A., Kobe, F., Ponimaskin, E., Zeug, A. and Neher, E. (2008). Analysis of FRET Signals in the Presence of Free Donors and Acceptors. *Biophys. J.* **94**, 986–1000.

Woehler, A. and Ponimaskin, E. (2009). G Protein - Mediated Signaling: Same Receptor, Multiple Effectors. *Curr. Mol. Pharmacol.* **2**, 237–248.

Woehler, A., Wlodarczyk, J. and Ponimaskin, E. G. (2008). Specific oligomerization of the 5-HT1A receptor in the plasma membrane. *Glycoconj. J.* **26**, 749–756.

Yelleswarapu, N. K., Tay, J. K., Fryer, W. M., Shah, M. A., Garcia, A. N., Cheng, J. P. and Kline, A. E. (2012). Elucidating the role of 5-HT1A and 5-HT7 receptors on 8-OH-DPAT-induced behavioral recovery after experimental traumatic brain injury. *Neurosci. Lett.* **515**, 153–156.

Zeug, A., Woehler, A., Neher, E. and Ponimaskin, E. G. (2012). Quantitative Intensity-Based FRET Approaches—A Comparative Snapshot. *Biophys. J.* **103**, 1821–1827.

Zoli, M., Agnati, L. F., Hedlund, P. B., Li, X. M., Ferré, S. and Fuxe, K. (1993). Receptor-receptor interactions as an integrative mechanism in nerve cells. *Mol. Neurobiol.* **7**, 293–334.

Figures

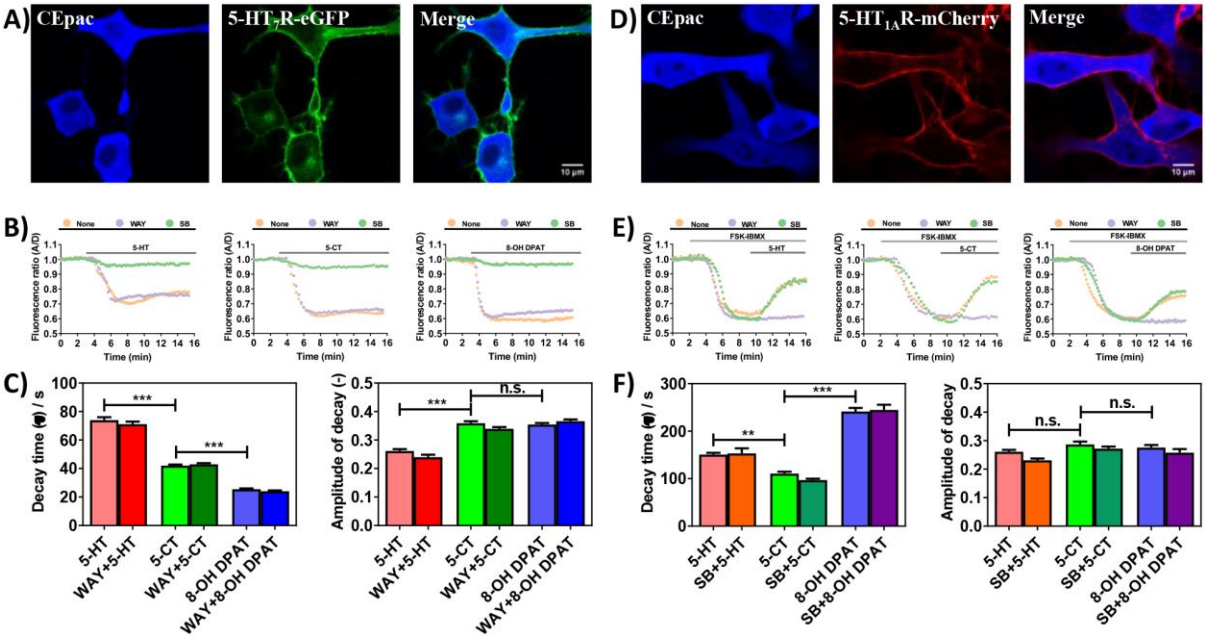

Figure 1: Agonist-induced changes in the fluorescence ratio correspond to receptor activation in N1E cells.

(**A, D**) Confocal visualization of transiently co-expressed cytosolic cAMP biosensor (blue) with either 5-HT_7R-eGFP (green, **A**) or 5-HT_{1A}R-mCherry (red, **D**) receptor exhibiting predominant localization to the plasma membrane. (**B, E**) Representative traces showing effects of the antagonists SB and WAY on the fluorescence ratio signal caused by agonists (5-HT, 5-CT and 8-OH-DPAT) (n≥50). Initial values of the fluorescence ratio were normalized. (**C, F**) Comparison of decay time and amplitude of decay evoked by 10 µM agonists in the absence and presence of 10 nM WAY and 100 nM SB for 5-HT_7R and 5-HT_{1A}R, respectively. Data are the means ± s.e.m.

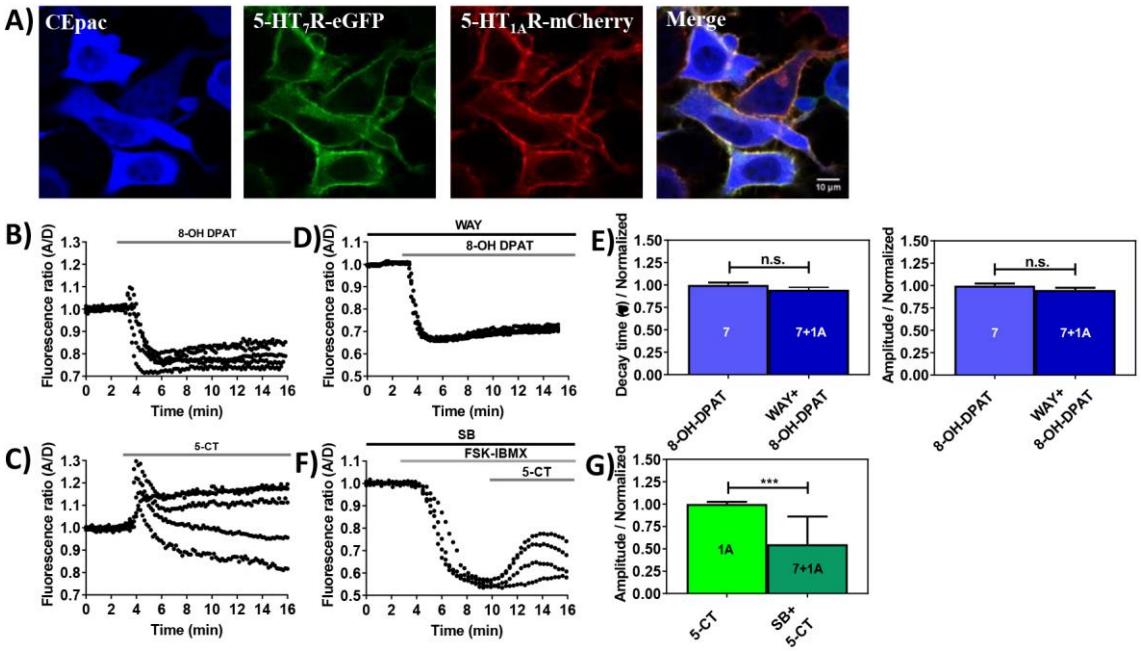

Figure 2: Agonist-induced changes in the fluorescence ratio correspond to receptor activation and blockage in N1E cells co-expressing the 5-HT$_7$ and 5-HT$_{1A}$ receptors.

(**A**) Confocal visualization of transiently co-expressed cytosolic cAMP biosensor CEpac (blue) and 5-HT$_7$R-eGFP (green) and 5-HT$_{1A}$R-mCherry (red) exhibiting predominant localization to the plasma membrane. (**B**) Representative traces showing change in the fluorescence ratio in response to the agonist 8-OH-DPAT (n≥50), (**C**) the agonist 5-CT (n≥50). (**D**) Representative traces of the fluorescence ratio in response to 8-OH-DPAT while pre-blocking 5-HT$_{1A}$R via WAY (n≥50). (**E**) Decay time t_1 and amplitude A_1 of the cAMP response induced by 5-HT$_7$R stimulation with 8-OH-DPAT in the absence or presence of 5-HT$_{1A}$R but blocked with WAY and applying fit model no1. (**F**) Representative traces of the fluorescence ratio in response to 5-CT in combination with pre-blocking 5-HT$_7$R with SB and FSK-IBMX stimulation (n≥50). (**G**) Change in ratio induced by 5-CT in the absence and the presence of 5-HT$_7$R but pre-blocked with SB. Amplitudes A_2 were obtained from fit model no2. Data are the means ± s.e.m.

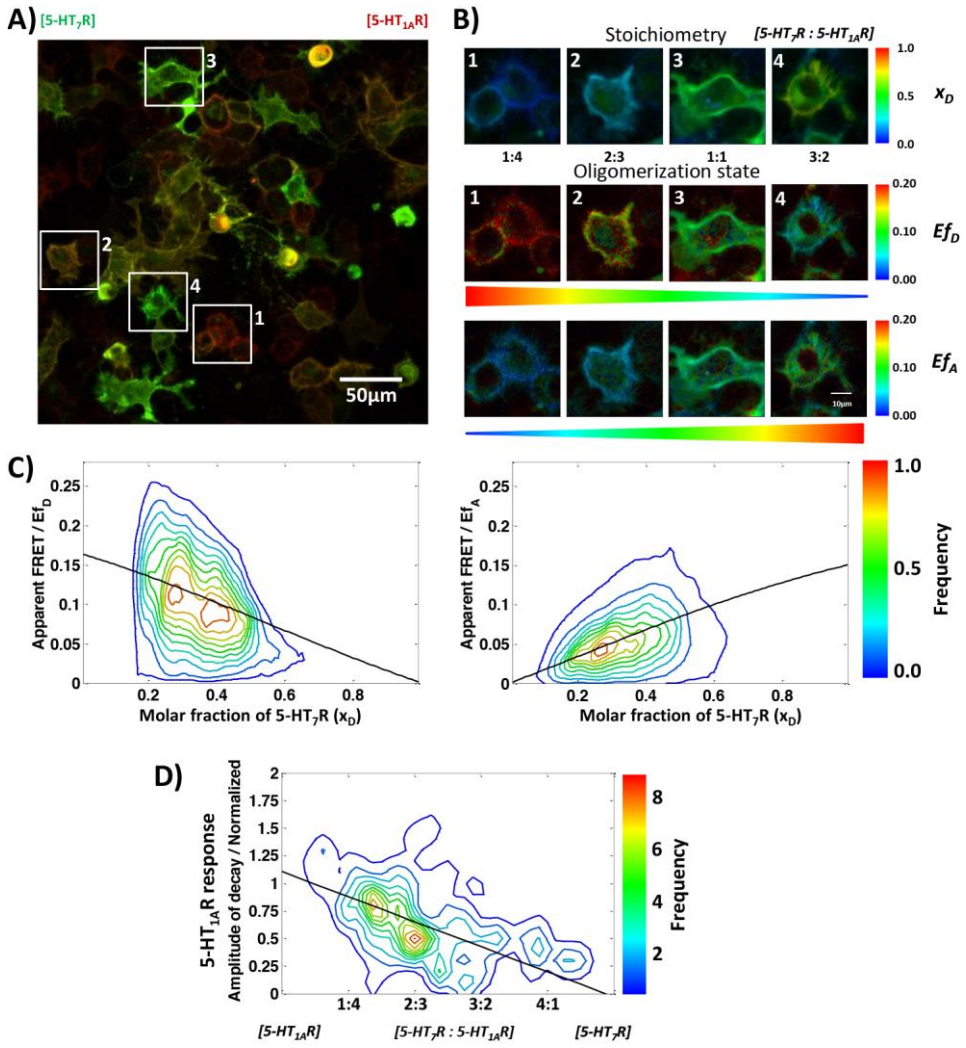

Figure 3. Hetero-oligomerization of 5-HT$_7$ and 5-HT$_{1A}$ receptors is correlated with cAMP kinetics.

(**A**) Images of FRET efficiency Ef_D and Ef_A and donor molar fraction x_D were obtained at single-cell level. (**B**) The inset shows various cells showing different $x_D = [D^t]/([D^t]+[A^t]) = [5\text{-}HT_7R]/([5\text{-}HT_7R] + [5\text{-}HT_{1A}R])$ values representing different ratios of receptors. Ef_D and Ef_A show the hetero-oligomer formation between 5-HT$_7$R and 5-HT$_{1A}$R. (**C**) Representative contour plots of 2D histogram of Ef_D and Ef_A are shown as functions of the donor molar fraction x_D and fitted by the fit model described in Renner *et al.* (Renner et al., 2012). (**D**) Contour plot of 2D histogram illustrating the relationship between the stoichiometry and cAMP response as the normalized amplitude A_2. Data were obtained from cells pre-blocked by SB and stimulated with FSK-IBMX and 5-CT ($n \geq 40$).

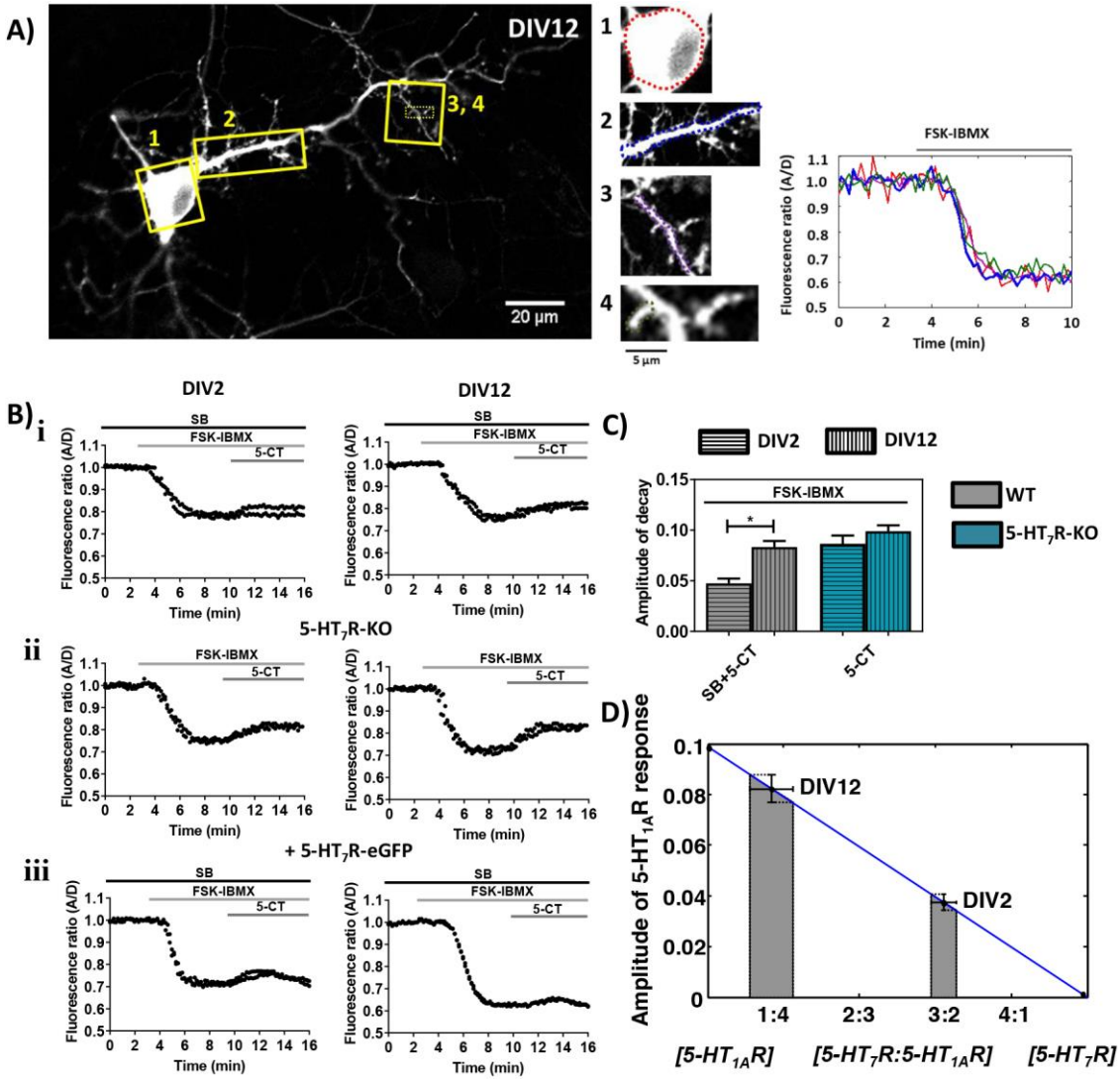

Figure 4. Relative endogenous expression levels of serotonergic receptors 5-HT$_7$ and 5-HT$_{1A}$ in hippocampal neurons *in situ* can be estimated from their cAMP kinetics.

(**A**) WT hippocampal neuron stimulation by FSK. Different regions (soma, dendrite and spines) in a DIV12 WT neuron indicating similar cAMP changes following FSK stimulation shown through representative traces. Initial values of the ratio traces were normalized. (**B**) Representative traces of fluorescence ratio changes in response to 8-OH-DPAT and 5-CT agonist measured in single neurons transiently expressing biosensor on DIV2 and DIV12. (**i**) Effect of pre-blocking 5-HT$_7$R with SB on the fluorescence ratio caused by FSK-IBMX and 5-CT; (**ii**) The change in the fluorescence ratio caused by FSK-IBMX and 5-CT in 5-HT$_7$R-KO neurons; (**iii**) Effect of pre-blocking 5-HT$_7$R with SB on the fluorescence ratio caused by FSK-IBMX and 5-CT in neurons transiently expressing 5-HT$_7$R-eGFP. (**C**) Comparison of the normalized amplitude of the fluorescent ratio data measured on DIV2 and DIV12 evoked by

5-CT in WT with SB pre-blocking and 5-HT_7R-KO neurons. Bars represent the increase in the fluorescence ratio following agonist exposure. (**D**) Correlation plot showing relationship between the receptor stoichiometry and normalized amplitude of cAMP response. Maximum amplitudes were obtained from the fluorescence ratio of 5-HT_7R-KO neurons stimulated with 5-CT transiently expressing only cAMP biosensor and have been set to 1 for maximal response. The 5-HT_7R:5-HT_{1A}R stoichiometry could be deduced from the amplitudes of WT neurons (cf. **Bi**, **C**). Data are the means ± s.e.m. of at least five separate experiments.

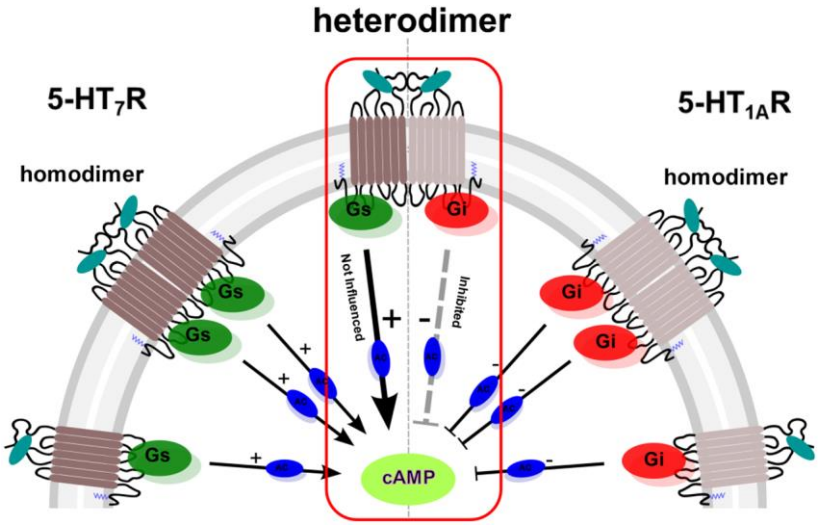

Figure 5. Oligomerization of serotonergic receptors 5-HT_7R and 5-HT_{1A}R impacts cAMP regulation following activation by agonist.

This model describes the relation between stoichiometry and receptor-mediated cAMP response following hetero-oligomerization. On heterodimer formation of both receptors, the 5-HT_{1A} receptor cAMP signaling pathway is inhibited, while on homodimerization and monomer formation, the respective cAMP pathways are not influenced. The colored arch-shaped symbols indicate agonist binding. A set of well-defined measurement protocols with parallel blocking and activation of specific receptor on co-expression were designed to measure cAMP responses for G_i- and G_s-coupled receptors. From simultaneous cAMP ratio and lux-FRET measurements, we were able to predict the stoichiometry of two receptors from the kinetics of intracellular cAMP level changes in WT neurons.

Supplementary data

Table S1: Primers used for cloning plasmids 5-HT_7R-eGFP and 5-HT_{1A}R-mCherry by using PCR-based approach: 5-HT_7R and 5-HT_{1A}R cDNAs were cloned in frame into pcDNA3.1 using BamH1 and EcoR1 cloning sites. eGFP and mCherry were fused to the N-terminal site of the 5-HT_7R and 5-HT_{1A}R and generated a functional GPCR, respectively. The following primers were used.

5-HT_7R-BamH1-for	5'-AAAGGATCCACCATGATGGACGTTAACAGCAG-3'
5-HT_7R-EcoR1-rev	5'-AAAGAATTCTGTATCATGACCTTTTTTCC-3'
5-HT_{1A}R-BamH1-for	5'-AAAGGATCCACCATGGATATGTTCAGTCTTGGCCAG-3'
5-HT_{1A}R-EcoR1-rev	5'-AAAGAATTCGCGGCAGAACTTGCACTTGATC-3'
mCherry-EcoR1-for	5'-AAAGGATCCACCATGGTGAGCAAGGC-3'
mCherry-Xba1-rev	5'-AAATCTAGACTTGTACAGCTCGTCCATGC-3'
eGFP-EcoR1-for	5'-AAAGGATCCACCATGCCCGAAGGCTACGTCCAG-3'
eGFP-Xba1-rev	5'-AAATCTAGAAGGGCGGACTGGGTGCTCAG-3'

Supplementary figures

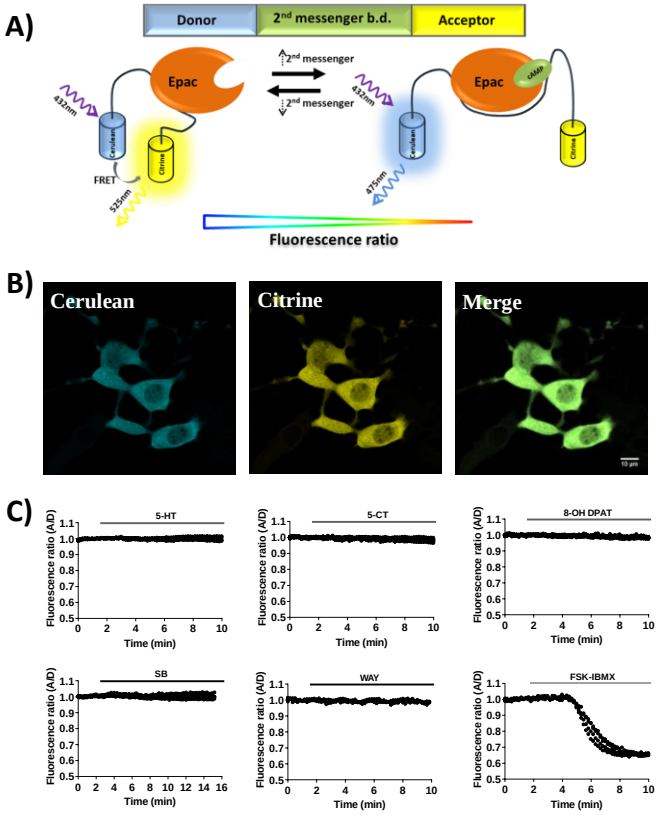

Figure S1. Effects of agonist and antagonist corresponding to biosensor responses in N1E cells.

(A) Schematic view of the cAMP FRET-based biosensor CEpac showing change in the acceptor / donor fluorescence (A/D) ratio upon cAMP binding. (B) Confocal visualization of transiently expressed cAMP biosensor (cyan-D and yellow-A part) exhibiting cytosolic expression throughout. (C) Representative traces showing effect of the specific antagonist for 5-HT7R and 5-HT1AR (SB and WAY) and 5-HTR agonists (5-HT, 5-CT and 8-OH-DPAT) on the fluorescence ratio in cells transiently expressing cAMP biosensor CEpac (n≥30), showing no change in the ratio, thus proving to be negative controls. As a positive control, 5 µM FSK in combination with 50 µM IBMX showed a strong decrease in normalized fluorescence ratio. Initial values of the fluorescence ratio were normalized to 1.

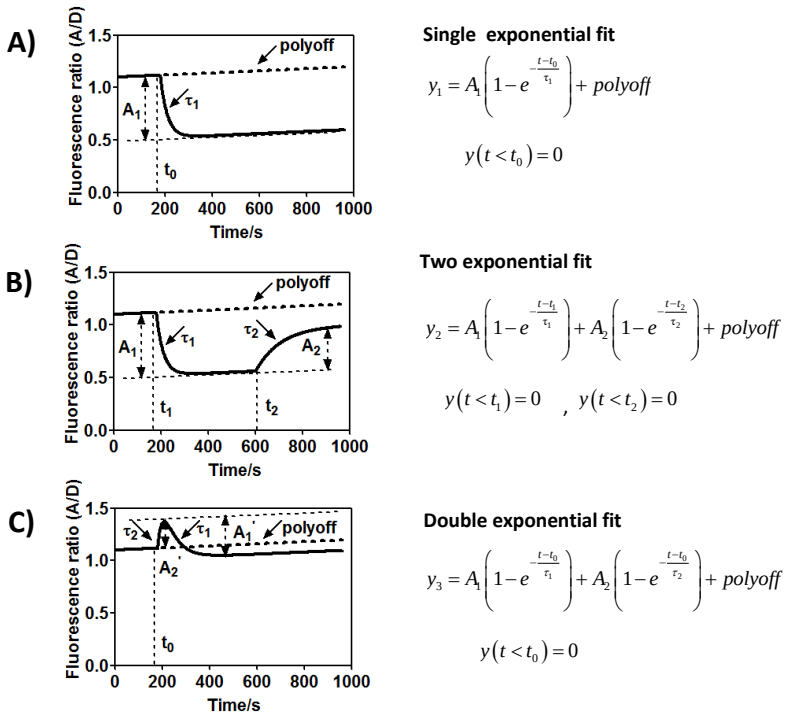

Figure S2. Exponential fitting models designed for cAMP signal kinetics.

(**A**) Fit model no1: single exponential fit with polynomial offset delivers decay time and amplitude at one time point. (**B**) Fit model no2: two exponential fits delivering two sets of amplitudes (A_1 and A_2) and decay times (τ_1 and τ_2) for cAMP regulation along with polynomial offset at two consecutive time points. (**C**) Fit model no3: double exponential fit combines two biological processes at one time point and delivers amplitude and decay time values, where the real values of the decay time and amplitude cannot be deduced because the two exponential functions are not orthogonal to each other in this case.

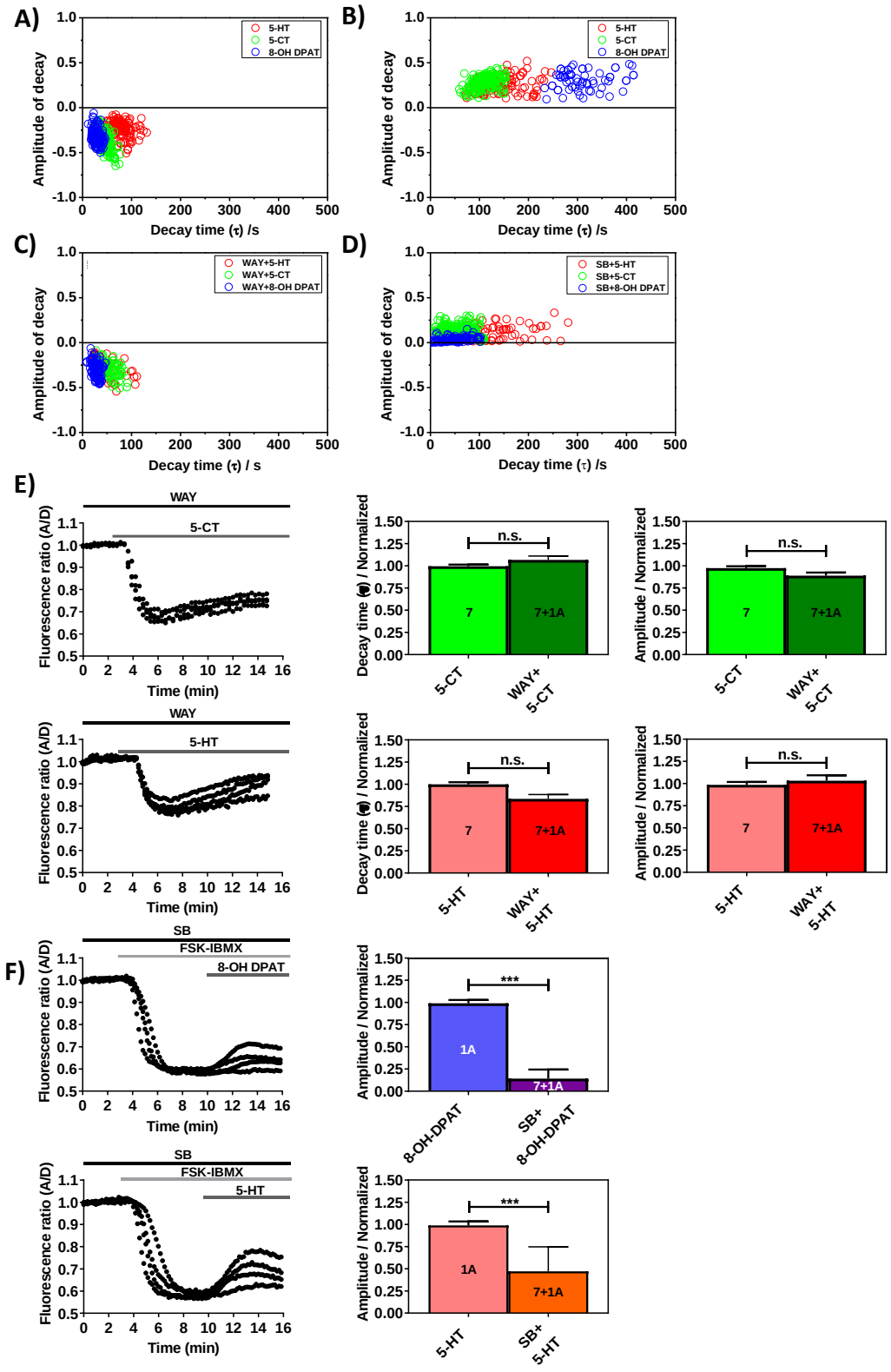

Figure S3. Different agonist-induced changes in the fluorescence ratio corresponding to receptor activation and blockage in N1E cells co-expressing 5-HT$_7$ and 5-HT$_{1A}$ receptors.

Scatter plot of amplitude of decay over decay time of results presented in this study. (**A**) N1E cells expressing 5-HT$_7$R, (**B**) 5-HT$_{1A}$R, (**C**) co-expressing 5-HT$_7$R and 5-HT$_{1A}$R, but pre-

blocked 5-HT_{1A}R with WAY and (**D**) co-expressing 5-HT_7R and 5-HT_{1A}R, but pre-blocked 5-HT_7R with SB. (**E-F**) representative traces and statistical evaluation of (**C**) and (**D**). The evaluation for WAY+8-OH-DPAT (**C, E**) is shown in Fig. 2E and for SB+5-CT (**D, F**) in Fig. 2G.

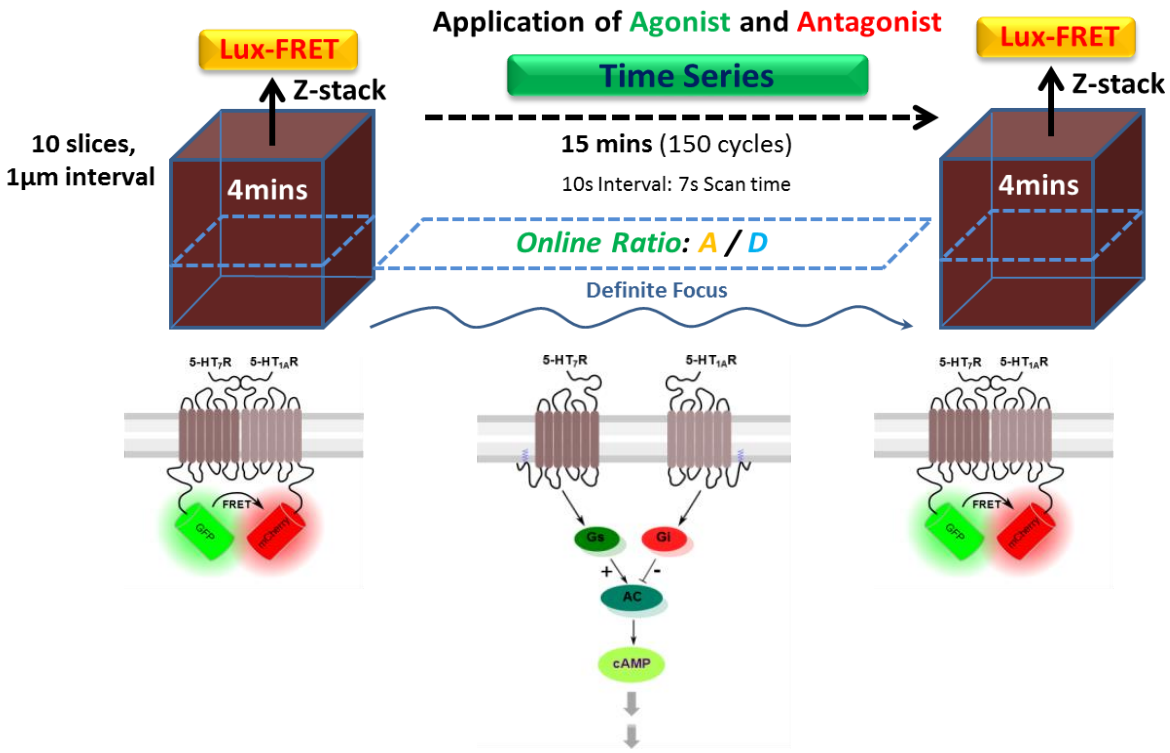

Figure S4. Schematic representation of experimental protocol and basic acquisition settings.

Time series fluorescence ratio (cycles) and lux-FRET (z-stack) measurement were performed sequentially as shown. In total, 25 min of the measurement protocol were set. During the experiments, 100 cycles with 10 s intervals along with continuous refocusing using the Zeiss "Definite Focus" were used. The number of frames before application (18-20 frames, 3 min) was kept constant. Z-stack containing 10 slices with 1.0 µm interval was set. Fluorescence ratio experiments applying FRET-based biosensor to measure intracellular cAMP level changes were performed for 5-HT_7R and 5-HT_{1A}R pathway on individual and co-expression.

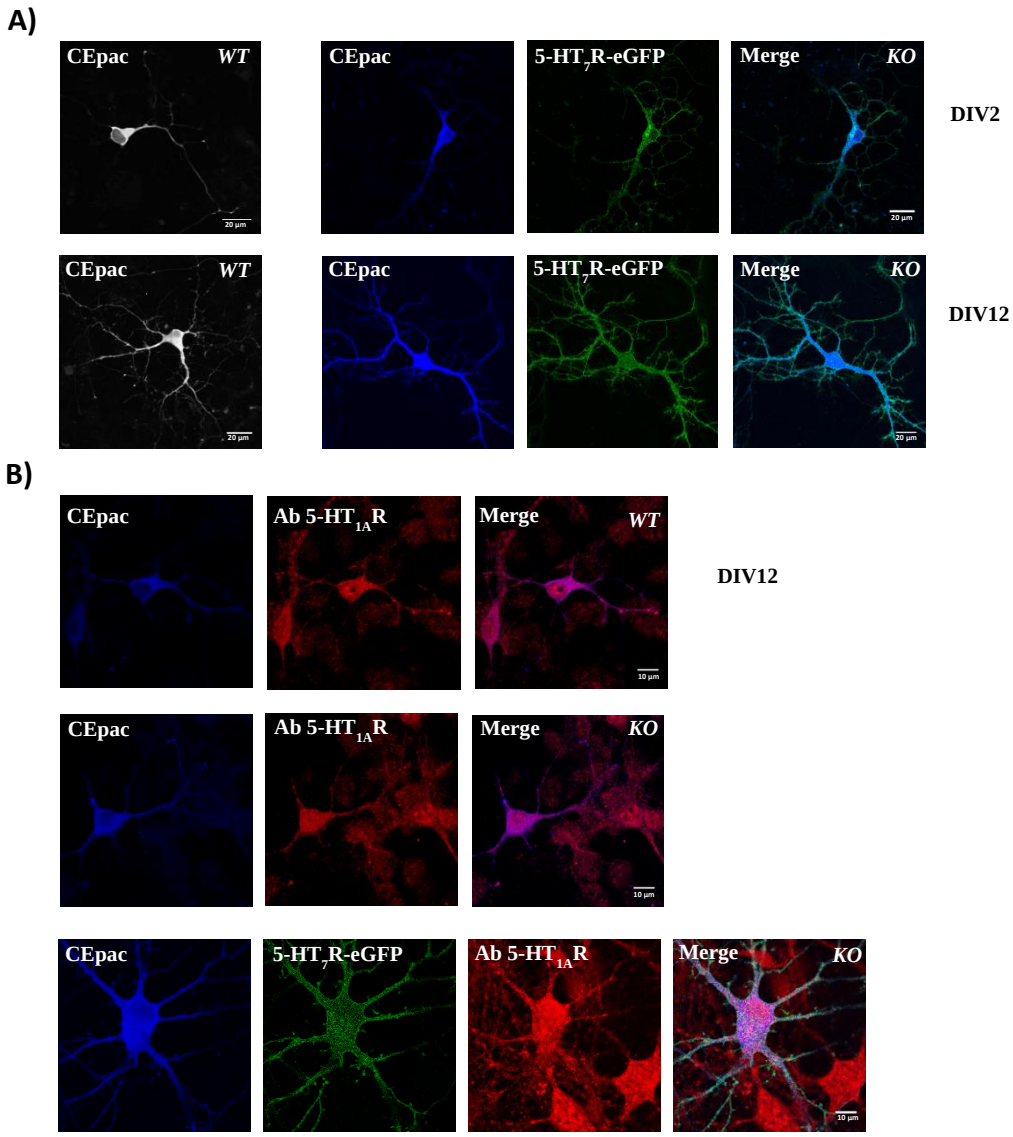

Figure S5. Confocal imaging of WT and 5-HT$_7$R-KO hippocampal neurons expressing cAMP biosensor and immunocytochemistry.

(**A**) Confocal imaging of cAMP biosensor expressed in WT and in addition expressing 5-HT$_7$R-eGFP receptor in 5-HT$_7$R-KO hippocampal neurons for DIV2 and DIV12. (**B**) Images of DIV12 WT and 5-HT$_7$R-KO neurons expressing cAMP biosensor and immunostained with anti-5-HT$_{1A}$R antibody shown individually and as a merge.

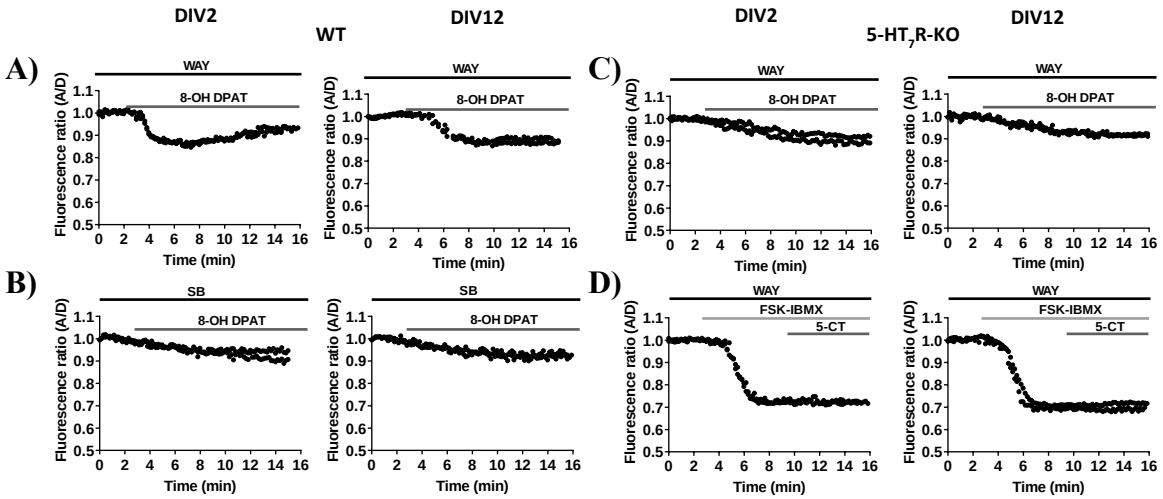

Figure S6. Agonist stimulation induced cAMP response in WT and 5-HT$_7$R-KO hippocampal neurons shows characteristic behavior as seen in N1E cells.

Representative traces of the fluorescence ratio changes in response to 8-OH-DPAT and 5-CT agonist measured in single immature and mature neurons transiently expressing biosensor (n≥5, N≥5) on DIV2 and DIV12. A) Effect of the antagonist WAY on the fluorescence ratio caused by 8-OH-DPAT blocking endogenous 5-HT$_{1A}$R. B) Effect of 8-OH-DPAT while blocking 5-HT$_7$R with SB. C) Effect of the 8-OH-DPAT on the fluorescence ratio while pre-blocking 5-HT$_{1A}$R with WAY. D) Changes in fluorescence ratio caused by FSK-IBMX and 5-CT and 5-HT$_{1A}$R blocked by WAY. A, B) WT neurons, C, D) 5-HT$_7$R-KO neurons.

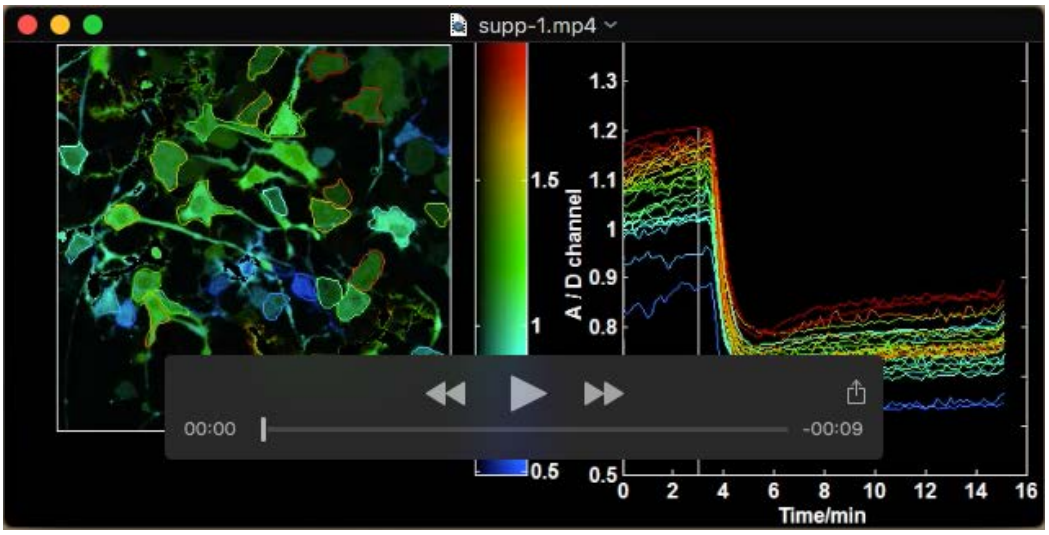

Movie 1: Confocal live cell imaging of N1E cells expressing 5-HT_7R and CEpac stimulated with 8-OH-DPAT which leads to an upregulation of cAMP level, elucidated by a ratio change of the FRET-based biosensor CEpac from red (high A/D ratio) to blue (low A/D ratio). Compare Fig. 1 in the main text and Movie 2.

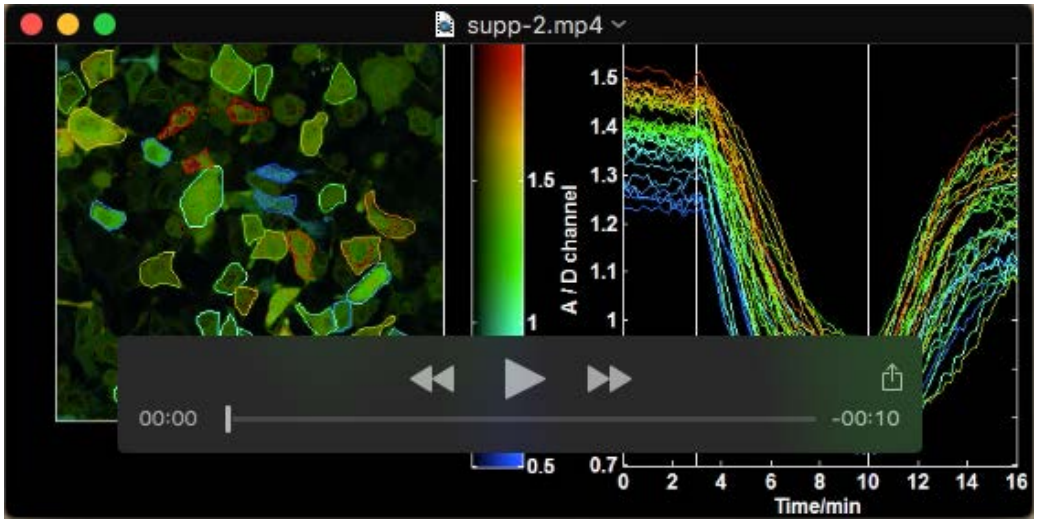

Movie 2: Confocal live cell imaging of N1E cells expressing 5-HT_{1A}R and CEpac stimulated with 5-CT after pre-stimulation with FSK and IBMX. The down-regulation of cAMP levels caused by 5-HT_{1A}R signaling via Gi was observed after the up-regulation of cAMP with FSK and IBMX. The cAMP concentration obtained from the FRET-based biosensor CEpac is color coded from blue (low [cAMP]) to red (low [cAMP]). Compare Fig. 1 in the main text and Movie 1.

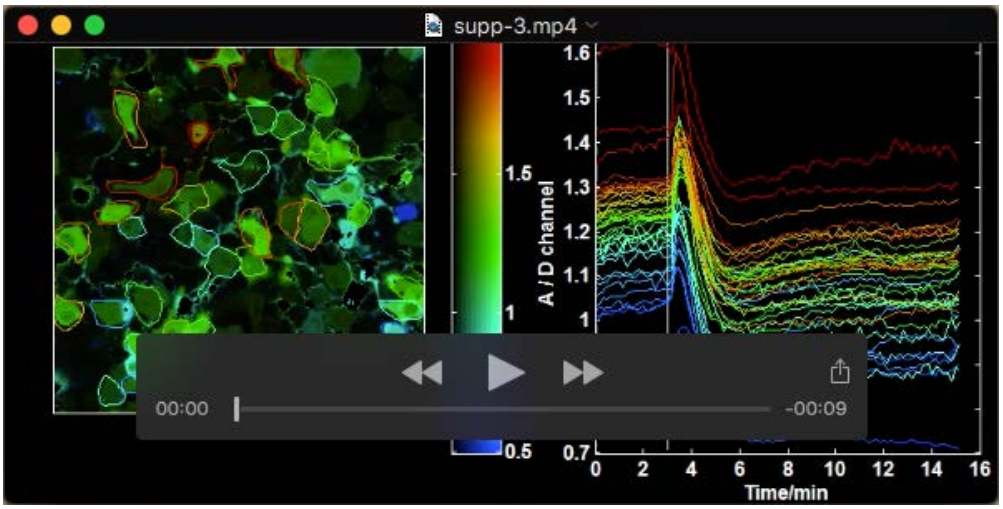

Movie 3: Confocal live cell imaging of N1E cells expressing 5-HT$_7$R, 5-HT$_{1A}$R and CEpac stimulated with 8-OH-DPAT cause overlaid cAMP responses of down- and up-regulation. The relative expression levels of 5-HTR is comparable from cell to cell (not shown). Compare Fig. 2 in the main text and Movies 1, 2.

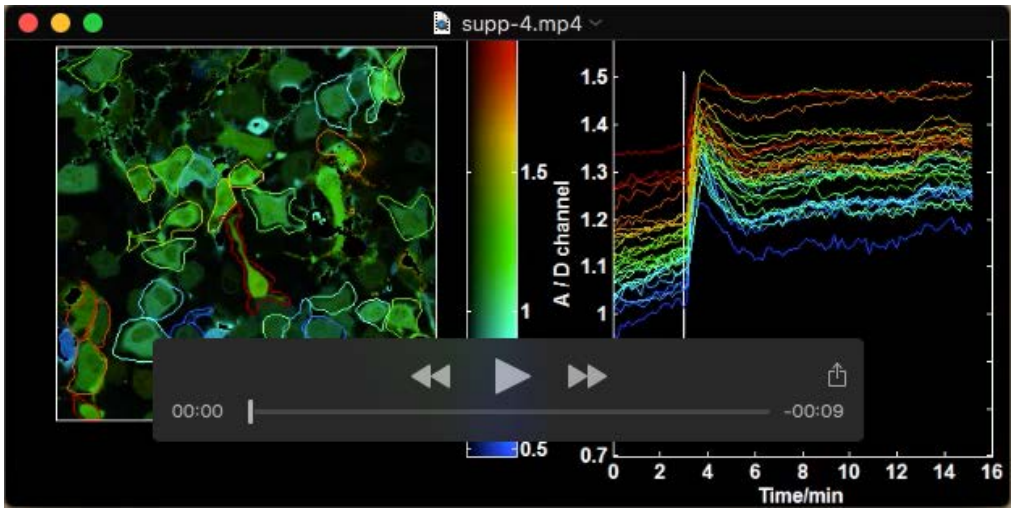

Movie 4: Confocal live cell imaging of N1E cells expressing 5-HT$_7$R, 5-HT$_{1A}$R and CEpac stimulated with 5-CT cause overlaid cAMP responses of down- and up-regulation. The relative expression levels of 5-HTR is comparable from cell to cell (not shown). Compare Fig. 2 in the main text and Movies 1-3.

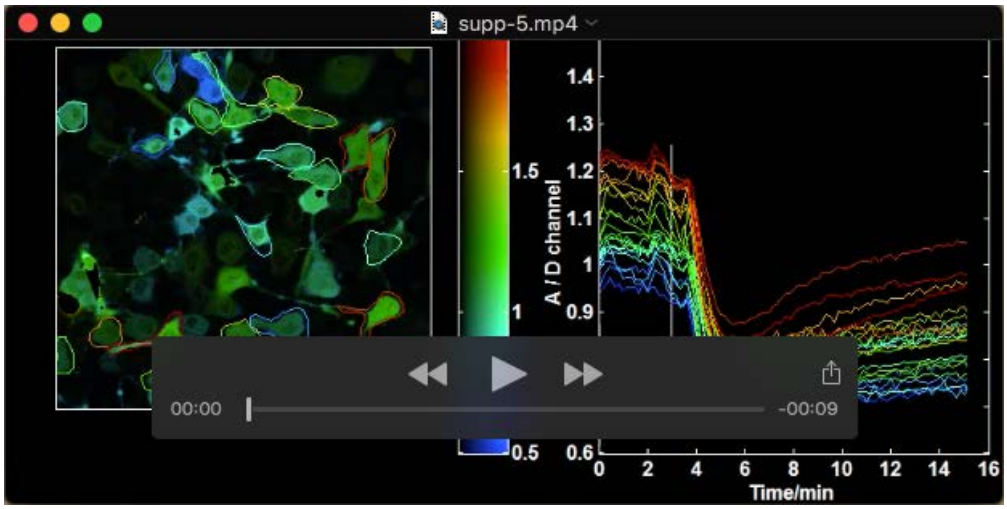

Movie 5: Confocal live cell imaging of N1E cells expressing 5-HT_7R, 5-HT_{1A}R and CEpac pre-blocked 5-HT_{1A}R with WAY and stimulated with 8-OH-DPAT. The relative expression levels of 5-HTR is deviating from cell to cell (not shown). Compare Fig. 2 in the main text and Movies 1-4.

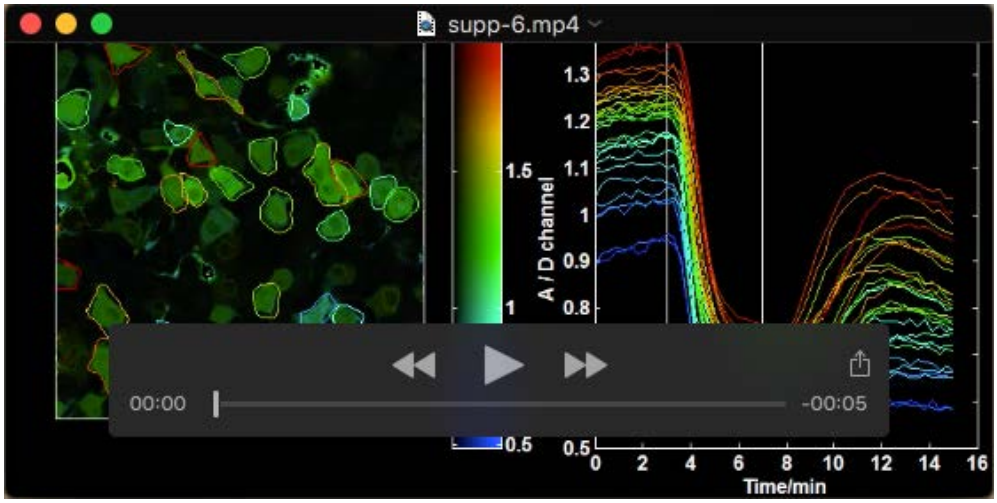

Movie 6: Confocal live cell imaging of N1E cells expressing 5-HT_7R, 5-HT_{1A}R and CEpac pre-blocked 5-HT_7R with SB and stimulated with 5-CT. The relative expression levels of 5-HTR is deviating from cell to cell (not shown). Compare Fig. 2 in the main text and Movies 1-5.